*Journal of Sound and Vibration* (2002) **252**(1), 83–113
doi:10.1006/jsvi.2001.4028, available online at http://www.idealibrary.com on IDEAL®

# A WAVENUMBER APPROACH TO MODELLING THE RESPONSE OF A RANDOMLY EXCITED PANEL, PART I: GENERAL THEORY

C. Maury, P. Gardonio and S. J. Elliott

*Institute of Sound and Vibration Research, University of Southampton, Southampton SO17 1BJ, England. E-mail: cm@isvr.soton.ac.uk*

(*Received* 15 *December* 2000, *and in final form* 30 *August* 2001)

Part I of this paper presents a self-contained analytical framework for determining the vibro-acoustic response of a plate to a large class of random excitations. The wavenumber approach is used, which provides an insight into the physical properties of the panel response and enables us to evaluate efficiently the validity of several simplifying assumptions. This formulation is used in Part II for predicting the statistical response of an aircraft panel excited by a turbulent boundary layer. In this paper, we first provide a general statement of the problem and describe how the spectral densities of the panel response can be obtained from an analysis of the system response to a harmonic deterministic excitation and a statistical model for the forcing field. The harmonic response of the system is then expanded as a series of the eigenmodes of the fluid-loaded panel and these fluid-loaded eigenmodes are approximated by a perturbation method. Then, we evaluate the conditions under which this series simplifies into a classical modal formulation in terms of the *in vacuo* eigenmodes.

To illustrate the use of a wavenumber approach, we consider three examples, namely, the vibro-acoustic response of a panel excited by an incidence diffuse acoustic field, by a fully developed turbulent flow and by a pressure field which is spatially uncorrelated from one point to another. Convergence properties of the modal formulations are also examined.



## 1. INTRODUCTION

In the wavevector–frequency approach, the properties of a space–time field are analyzed in terms of the spatial and temporal Fourier variables of the field. The method arises from a cross-fertilization among several disciplines such as fluid dynamics (analysis of turbulent flows), vibro-acoustics (fluid–structure interaction problems) and signal processing (spectral analysis of random fields). A number of studies have used the wavevector–frequency analysis, which is reviewed by Strawderman [1], who also presents a self-contained and general description of this theory.

This approach has two main advantages. First, it enhances the analytical tractability of the problem and provides complete or partial closed-form solutions which can considerably reduce the computational effort. Second, the wavevector–frequency analysis allows a physical interpretation of the problem, especially in terms of filtering effect of the system, but also expresses how some characteristics of the system are distributed among the wavevector and frequency variables, i.e., the rate of change of these characteristics with respect to distance and time.

Interest in the wavevector–frequency analysis has grown with studies concerned with the design of filters used to measure the wavevector–frequency content of a spatially distributed

0022-460X/02/$35.00 

stationary random process, such as the wall-pressure fluctuations beneath a turbulent boundary layer, either with an array of transducers [2, 3] or a planar elastic structure [4, 5]. Wavenumber–frequency measurements have provided useful information about the energy content of the wall-pressure field in the low wavenumber domain and thus, complement the space–time correlation measurements already obtained by Corcos [6], which are completely valid only at or near the convective wavenumber. Various empirical or semi-empirical turbulent boundary layer models have thus been formulated in the wavevector–frequency domain with different ranges of validity [7–9].

These models are appropriate to predict the vibrating and acoustic response of a structure excited by a turbulent flow with one dimension parallel to the streamwise direction of the flow [10–12]. The vibro-acoustic response can then be interpreted as the result of passing the excitation spectrum through a three-dimensional filter (frequency and two wavenumber components) characterized by a *sensitivity* function which only depends on the geometrical and mechanical properties of the structure. The visualization on a graph of the spectral contents of both the excitation and the sensitivity function provides a straightforward interpretation for the spectral distribution of the system response.

An important aspect of this theory is the required accuracy for both the excitation model and the wavenumber–frequency sensitivity function of the structure and their relationship. In some infinite structures, for which the sensitivity function is known exactly, the accuracy of the excitation completely determines the accuracy with which the system response can be calculated. However, the accuracy of the numerical approximations used to determine the sensitivity function for finite and complex structures relies on the validity of the simplifying assumptions for the model, and also, on the quality of the approximation method (convergence, consistence, etc). Several studies have already considered the influence of a turbulent excitation model on the system response [13, 14].

In this paper, we are primarily concerned with the *a priori* determination, for a given model of random excitation, of the required accuracy of the sensitivity function and its influence on the system response, particularly the number of modes used in the expansion of the structural response. The second objective of this study is to present a method that enables different types of general random excitations to be accounted for. A large class of random processes can be considered as *weakly stationary*, i.e., when their moment functions only up to order 2 depend on the difference in the parameter values indexing the process. If the parameter stands for a spatial variable, then the term "stationary" is commonly replaced by the term "homogeneous". An example of a weakly stationary and weakly homogeneous random process is the wall-pressure fluctuations induced by a turbulent boundary layer over the fuselage panel of an aircraft or a submarine under cruise conditions, as long as we consider a portion of the flow far away from surface irregularities [15]. Another example is the structural or fatigue response of an automobile during a journey, in which it travels at a constant speed on a road with a surface roughness that generates weakly stationary vibrations of the car body (among other sources of vibrations) [16]. In general, the conditions for the existence of the spectral decomposition of such random processes are not satisfied. Hence, we propose a general analysis based on the use of the impulse response method [17] to determine the statistical properties of the system response to a class of weakly stationary processes, but that could also account, with a few modifications, for non-stationary processes.

This paper is organized as follows. In section 2, we describe a self-contained theoretical model of wavevector–frequency analysis for the prediction of the sound transmitted through a baffled panel excited by a random process in time and space. It will be established that the statistical properties of the panel response depend on the statistics of the excitation through the response of the fluid-loaded panel to an ensemble of harmonic plane waves

scaled on each contributing wavevector. In section 3, a series expansion in terms of the fluid-loaded eigenmodes of the panel will be used to solve the corresponding set of harmonic problems and quantitative criteria will be derived under which the usual simplifications, such as neglecting the fluid-loading effects or assuming the statistical independence of the eigenmodes, are valid. Finally, numerical example are presented in section 4 for different types of excitations and the convergence properties of the approximation method for the sensitivity function are covered in appendix A.

## 2. GENERAL STATEMENT OF THE PROBLEM

In the three-dimensional domain $R^3$, we consider the Cartesian set of co-ordinates $(O; x, y, z)$. A thin elastic (or visco-elastic) plate of length $a$, of width $b$ and of constant thickness $h \ll (a, b)$, occupies the space domain defined by

$$\{\mathbf{x} = (x, y, z): 0 < x < b,\ 0 < y < a,\ -h/2 < z < h/2\}. \tag{1}$$

For simplicity, the plate is assumed to be homogeneous and isotropic. Its vibrations are modelled by the *Kirchhoff's thin plate equation* which is the simplest approximation that can be established for a plate. All the structural quantities will therefore, be defined over the mean surface $\mathbf{\Sigma}(z = 0)$ of the plate. Along its boundary $\partial\mathbf{\Sigma}$, an external normal vector $\mathbf{n}$ can be defined almost everywhere. The complement $\mathbf{\Sigma}'$ of $\mathbf{\Sigma}$ is a perfectly rigid baffle.

The mechanical characteristics of the plate are: a bending stiffness $D = Eh^3/12(1 - \nu^2)$ and a mass per unit area $m = \rho h$ where $E$, $\nu$ and $\rho$ are the Young's modulus of elasticity, the Poissons' ratio and the density of the material. The mechanical damping is either due to internal dissipation mechanisms in the plate material or to energy losses through the plate boundaries. The "hereditary" damping formulation used by Preumont [18] provides a general model from which the hysteretic and viscous damping formulations can be deduced. We will account for the tensioning effects through lateral and longitudinal positive restoring forces terms $N_x$ and $N_y$ acting in the plane of the undeformed middle surface of the plate.

The baffled plate separates two domains $\mathbf{\Omega}^+(z > 0)$ and $\mathbf{\Omega}^-(z < 0)$ which both contain perfect fluids which are characterized by the densities $\rho^+$ and $\rho^-$ with the corresponding sound velocities $c^+$ and $c^-$. The forcing field is described by a force density which depends randomly on space and time variables. The plate vibrations induced and the acoustic pressure radiated in both fluid domains are also described by a random process.

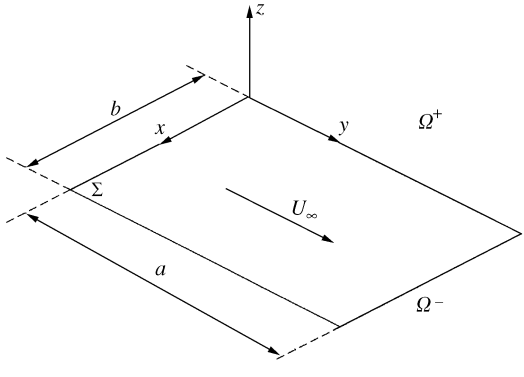


Figure 1. The panel configuration with co-ordinate system.

In the case of a convecting random pressure field (turbulent boundary layer excitation), the $y$-axis is parallel to a flow moving in the domain $\mathbf{\Omega}^+$ with the constant speed $U_\infty$ (see Figure 1). The panel is then excited by the wall-pressure fluctuations induced by a turbulent boundary layer developed along the interface fluid/baffled plate.

### 2.1. HYPOTHESIS

We assume that the deflections are small in comparison to the thickness of the plate and so, we restrain our model to the linear domain where the influence of the mid-plane stretching on the tension terms can be neglected.

The following assumptions are specific to a turbulent flow excitation. First, the turbulent boundary layer is assumed to be fully developed when exciting the plate. Second, we will consider that the wall-pressure fluctuations are not affected by the vibrations of the plate, i.e. that the forcing term is not modified by the panel response [19]. This assumption holds as long as the flow-induced displacements, are much smaller than the characteristic length scales of the flow and as long as we are further downstream from the transitional boundary layer so that the flow is robust to small perturbations due to the plate vibrations. Thus the turbulent excitation term is modelled by the wall-pressure fluctuations that would be observed on a smooth rigid wall, also called the *blocked pressure* $p_b$. This approximation makes the problem more tractable. An exact approach, based upon the Lighthill–Curle theory of aerodynamic sound generation [20], would be to consider the plate excited by the acoustic pressure generated by moving acoustic sources and with an integral representation which requires the solution of the entire flowfield. Third, we assume that the sound pressure radiated in $\mathbf{\Omega}^-$ is not significantly affected by the fluid flow in $\mathbf{\Omega}^+$. So, for the acoustic wave propagation in $\mathbf{\Omega}^+$, we consider that the fluid is at rest. However, we limit our predictions to Mach numbers lower than 0·8, as the external radiation damping can still be considered as negligible with respect to the internal radiation damping and the mechanical damping of the plate in this Mach number range. For transonic and supersonic Mach numbers, it can be shown that the aeroelastic structural acoustic coupling has a significant influence on the sound power inwardly radiated [21].

In summary, we have to evaluate the vibro-acoustic response of a plate in contact with a quiescent fluid and excited by a force density with known statistical properties.

### 2.2. GOVERNING EQUATIONS

Let $w(\mathbf{x}; t)$ be the instantaneous flexural displacement of the mean surface of the plate at the point $\mathbf{x}$ of co-ordinates $(x, y, 0)$ and at the time $t$; let $p^+(\mathbf{z}; t)$ and $p^-(\mathbf{z}; t)$ stand for the acoustic pressure fields at the points $\mathbf{z}$ of co-ordinates $(x, y, z \geqslant 0)$ and $(x, y, z \leqslant 0)$, respectively, in $\mathbf{\Omega}^+$ and $\mathbf{\Omega}^-$ and at the time $t$. The pressure step $p_S(\mathbf{x}; t)$ across the plate is defined by

$$p_S(\mathbf{x}; t) = p_S(x, y, 0; t) = \lim_{z \to 0} [p^+(x, y, z; t) - p^-(x, y, -z; t)], \quad z > 0. \tag{2}$$

The functions $w(\mathbf{x}; t)$, $p^+(\mathbf{z}; t)$ and $p^-(\mathbf{z}; t)$ satisfy, for each realization of the process, the following system of equations:

$$\left( \mathscr{L}_P + \theta^*_{(t)} \frac{\partial \mathscr{L}'_P}{\partial t} + m \frac{\partial^2}{\partial t^2} \right) w(\mathbf{x}; t) = - p_{b,\mathbf{\Sigma}}(\mathbf{x}; t) - p_S(\mathbf{x}; t), \quad \mathbf{x} \in \mathbf{\Sigma}, \tag{3}$$

where

$$\mathscr{L}_P(w) = D\left(\frac{\partial^2 w}{\partial x^2} + \frac{\partial^2 w}{\partial y^2}\right)^2 - N_x \frac{\partial^2 w}{\partial x^2} - N_y \frac{\partial^2 w}{\partial y^2},$$

$$\left(\nabla^2 - \frac{1}{c_\pm^2}\frac{\partial^2}{\partial t^2}\right) p^\pm(\mathbf{z}; t) = 0, \quad \mathbf{z} \in \mathbf{\Omega}^\pm, \tag{4}$$

$$\rho_\pm \frac{\partial^2 w}{\partial t^2}(\mathbf{x}; t) + \frac{\partial p^\pm}{\partial z}(\mathbf{x}; t) = 0, \quad \mathbf{x} \in \mathbf{\Sigma}, \tag{5}$$

$$\frac{\partial p^\pm}{\partial z}(\mathbf{x}; t) = 0, \quad \mathbf{x} \in \mathbf{\Sigma}', \tag{6}$$

$$w(\mathbf{x}; 0) = \frac{\partial w}{\partial t}(\mathbf{x}; 0) = 0, \quad \mathbf{x} \in \mathbf{\Sigma}, \tag{7}$$

$$p^\pm(\mathbf{x}; 0) = \frac{\partial p^\pm}{\partial t}(\mathbf{x}; 0) = 0, \quad \mathbf{x} \in \mathbf{\Omega}^\pm, \tag{8}$$

$$\text{boundary conditions for } w \text{ on } \partial\mathbf{\Sigma}, \tag{9}$$

$$\text{outgoing wave conditions for } p^\pm \text{ in } \mathbf{\Omega}^\pm. \tag{10}$$

Equation (3) governs the structural response of the fluid-loaded plate under membrane tensions and excited by the total acoustic pressure field induced by both the forcing pressure field $p_{b,\mathbf{\Sigma}}(\mathbf{x}; t) = b_{\mathbf{\Sigma}}(\mathbf{x}) p_b(\mathbf{x}; t)$, where $b_{\mathbf{\Sigma}}(\mathbf{x})$ is the space-limiting function associated to the plate domain, and the acoustic pressure discontinuity $p_S$. The hereditary damping term $\theta^*_{(t)} \partial \mathscr{L}'_P(w)/\partial t$ involves a convolution integral with respect to time between $\theta$, the heredity function, and the plate velocity passed through a spatial operator $\mathscr{L}'_P$ [18]. These quantities will be specified in the next paragraph according to the damping mechanism.

This equation is completed by initial conditions (7) and local boundary conditions (9) satisfied by $w$ along its entire periphery $\partial\mathbf{\Sigma}$. The simplest one corresponds to the case of a simply supported plate ($w = \partial_n^2 w = 0$ on $\partial\mathbf{\Sigma}$) or the case of a clamped plate ($w = \partial_n w = 0$ on $\partial\mathbf{\Sigma}$). But, boundary integral representations of $w$ can take any other conditions into account [22].

The acoustic pressure fields $p^+$ and $p^-$ satisfy the homogeneous d'Alembert equations (4), respectively, in the fluid domains $\mathbf{\Omega}^+$ and $\mathbf{\Omega}^-$, the homogeneous Neumann boundary condition (6) on the baffle, the initial conditions (8) and a condition of energy conservation (10) at infinity. Since the fluid is assumed to be perfect and at rest, equation (5) expresses the continuity condition between the normal acceleration of a point vibrating on the structure and a fluid particle at its neighbourhood.

The set of equations (2–10) governs the vibrating motion of the fluid-loaded baffled plate stressed by in-plane tensions, initially at rest and excited by a random field.

### 2.3. GREEN FUNCTION REPRESENTATION OF THE DISPLACEMENT OF THE FLUID-LOADED PLATE

The basic methodology developed in this subsection and in the next enables one to evaluate the wavevector–frequency response of space-limited, time-invariant linear systems.

It leads to the classical expressions (29, 36) for the spectral densities of the stochastic fields in the wavenumber domain. Such expressions have already been used in similar studies [10, 13]. However, for the sake of completeness, we will describe the main steps of the proof. Moreover, many authors [11, 23, 24] have directly solved the time-Fourier transform of the set of equations (2–10) although, according to the author in references [16, 25], the Fourier transform of some random processes, such as the weakly stationary fields, is not defined, at least in a classical way. As an alternative, our approach does not require such a transformation. But, since both approaches lead to the same result, it is instructive to show their correspondence (see Part II, Appendix A.3. in the case of a TBL excitation).

Introducing the space–time impulse response $\gamma(\mathbf{x}, \mathbf{x}'; t)$ of the system fluid/baffled plate, the principle of superposition applied to a space-varying time-invariant linear system (see equations (2–10)) leads to an integral representation of the displacement of the fluid-loaded plate in terms of the random excitation $p_b$, as follows [17, Chapter 7.1]:

$$w(\mathbf{x}; t) = \left(\gamma \underset{(\mathbf{x}', t)}{*} p_{b,\Sigma}\right)(\mathbf{x}; t) = \int_0^t \iint_{\Sigma} \gamma(\mathbf{x}, \mathbf{x}'; t - \tau) p_b(\mathbf{x}'; \tau)\, \mathrm{d}\tau\, \mathrm{d}^2\mathbf{x}', \tag{11}$$

where $\underset{(\mathbf{x}', t)}{*}$ denotes a convolution product with respect to space and time variables and $\gamma(\mathbf{x}, \mathbf{x}'; t)$, also called the Green function of the system in the physical domain, can be defined as the inverse time-Fourier transform of the Green function $\gamma(\mathbf{x}, \mathbf{x}'; \omega)$, in the space–frequency domain:

$$\gamma(\mathbf{x}, \mathbf{x}'; t) = \frac{1}{2\pi} \int_{-\infty}^{+\infty} \gamma(\mathbf{x}, \mathbf{x}'; \omega) \mathrm{e}^{\mathrm{j}\omega t}\, \mathrm{d}\omega. \tag{12}$$

$\gamma(\mathbf{x}, \mathbf{x}'; \omega)$ satisfies the following system of equations:

$$(\mathscr{L}_P + \mathrm{j}\omega\theta(\omega)\mathscr{L}'_P - m\omega^2)\gamma(\mathbf{x}, \mathbf{x}'; \omega) = -\delta_{\mathbf{x}'}(\mathbf{x}) - p_S(\mathbf{x}, \mathbf{x}'; \omega), \quad (\mathbf{x}, \mathbf{x}') \in \boldsymbol{\Sigma}, \tag{13}$$

$$(\boldsymbol{\Delta} + k_{\pm}^2) p^{\pm}(\mathbf{z}, \mathbf{x}'; \omega) = 0, \quad (\mathbf{z}, \mathbf{x}') \in \boldsymbol{\Omega}^{\pm} \times \boldsymbol{\Sigma}, \quad k_{\pm} = \omega / c_{\pm}, \tag{14}$$

$$\frac{\partial p^{\pm}}{\partial z}(\mathbf{x}, \mathbf{x}'; \omega) = \rho_{\pm} \omega^2 \gamma(\mathbf{x}, \mathbf{x}'; \omega), \quad (\mathbf{x}, \mathbf{x}') \in \boldsymbol{\Sigma}, \tag{15}$$

$$\frac{\partial p^{\pm}}{\partial z}(\mathbf{x}, \mathbf{x}'; \omega) = 0, \quad (\mathbf{x}, \mathbf{x}') \in \boldsymbol{\Sigma}', \tag{16}$$

$$\text{boundary conditions for } \gamma(\mathbf{x}, \mathbf{x}'; \omega) \text{ when } \mathbf{x} \in \partial\boldsymbol{\Sigma}, \tag{17}$$

$$\text{Sommerfeld conditions for } p^+ \text{ and } p^-, \tag{18}$$

where $p^{\pm}(\mathbf{z}, \mathbf{x}'; \omega)$ is the sound pressure radiated at the point $\mathbf{z}$ in $\boldsymbol{\Omega}^{\pm}$ due to a harmonic point force $\delta_{\mathbf{x}'}(\mathbf{x})\mathrm{e}^{\mathrm{j}\omega t}$ acting normally on the plate at the point $\mathbf{x}'$; $\delta_{\mathbf{x}'}(\mathbf{x}) = \delta_{\mathbf{x}'}(x)\delta_{\mathbf{y}'}(y)$ is the Dirac delta function at the point $\mathbf{x}'$ of co-ordinates $(x', y', 0)$; $p_S(\mathbf{x}, \mathbf{x}'; \omega)$ is the pressure step across the plate at the point $\mathbf{x}$ on $\boldsymbol{\Sigma}$. Physically, $\gamma(\mathbf{x}, \mathbf{x}'; \omega)$ represents the flexural response,

i.e., the out-of-plane displacement, at the point $\mathbf{x}$ on $\mathbf{\Sigma}$, of a baffled plate in contact with two fluids occupying the semi-infinite domains $\mathbf{\Omega}^{\pm}$ and excited by a harmonic unit point force. $\omega$ is the angular frequency and $k_{\pm}$ is the acoustic wavenumber in each fluid domain. In equation (13), if we assume that the mechanical damping is hysteretic, then $\theta(\omega)$ is given b $\eta\,\mathrm{sign}(\omega)/\omega$ where $\eta$ is the hysteretic loss factor and $\mathscr{L}'_P = \mathscr{L}_P$ [26]. Assuming a viscous damping, the heredity function is constant and $\mathscr{L}'_P$ is the identity operator [18].

## 2.4. VIBRO-ACOUSTIC RESPONSE OF AN ELASTIC PANEL TO A SPACE AND TIME STOCHASTIC EXCITATION

In this section, we will first derive the wavevector–frequency spectrum associated to the vibro-acoustic response of the baffled plate excited by a space-limited forcing pressure field. Then we will discuss the advantages of a wavenumber–frequency formulation.

### 2.4.1. *Spectral density of the structural response*

The forcing term is modelled by the stochastic field $p_b(\mathbf{x}; t)$ the statistics of which are usually assumed to be both stationary and homogeneous up to order 2 [15]. Thus, the *auto-correlation function* $R_{p_b p_b}$ of the random process has the functional form

$$R_{p_b p_b}(\mathbf{\Xi}; \tau) = E[p_b(\mathbf{x}; t) p_b(\mathbf{x} + \mathbf{\Xi}; t + \tau)], \tag{19}$$

where $\mathbf{\Xi} = \mathbf{x}' - \mathbf{x}$ is the spatial separation vector, $\tau$ is the time difference and $E$ denotes the mathematical expectation (or space–time average). The *wavevector–frequency spectrum* of the excitation pressure $p_b(\mathbf{x}; t)$ is denoted $S_{p_b p_b}(\mathbf{k}; \omega)$ and is defined as the space–time Fourier transform of the auto-correlation function $R_{p_b p_b}(\mathbf{\Xi}; \tau)$; that is, in terms of the *space–frequency spectrum*, $S_{p_b p_b}(\mathbf{\Xi}; \omega)$ of the excitation pressure;

$$S_{p_b p_b}(\mathbf{k}; \omega) = \iint_{\Sigma} S_{p_b p_b}(\mathbf{\Xi}; \omega) \mathrm{e}^{\mathrm{j}\mathbf{k}\mathbf{\Xi}} \mathrm{d}^2\mathbf{\Xi} \tag{20}$$

and

$$S_{p_b p_b}(\mathbf{\Xi}; \omega) = \int_{-\infty}^{+\infty} R_{p_b p_b}(\mathbf{\Xi}; t) \mathrm{e}^{-\mathrm{j}\omega t} \mathrm{d}t, \tag{21}$$

where the wavevector $\mathbf{k} = (k_x, k_y)$ and the angular frequency $\omega$ are the Fourier dual variables, respectively, of $\mathbf{\Xi}$ and $\tau$.

Because we consider a spatially non-uniform system, the Green function $\gamma(\mathbf{x}, \mathbf{x}'; t)$, defined by equations (31–18), depends on the absolute spatial variable $\mathbf{x}$. Thus, the statistics of the displacement field given by (11) are stationary, but non-homogeneous. It follows that the *auto-correlation function* $R_{ww}$ associated with the plate displacement is given by

$$R_{ww}(\mathbf{x}, \mathbf{x}'; \tau) = E[w(\mathbf{x}'; t') w(\mathbf{x}, t' + \tau)]. \tag{22}$$

Substitution of equation (11) into definition (22) yields an integral representation of the auto-correlation function $R_{ww}$ in terms of the auto-correlation function $R_{p_b p_b}$ for the

excitation field:

$$R_{ww}(\mathbf{x}, \mathbf{x}'; t) = \int_{-\infty}^{+\infty}\int_{-\infty}^{+\infty} \iint_{\Sigma}\iint_{\Sigma} \gamma(\mathbf{x}, \mathbf{x}''; t-\tau) R_{p_b p_b}(\mathbf{x}''' - \mathbf{x}''; \tau' - \tau) \times \gamma(\mathbf{x}', \mathbf{x}'''; t-\tau')\, \mathrm{d}^2\mathbf{x}'''\, \mathrm{d}^2\mathbf{x}''\, \mathrm{d}\tau'\, \mathrm{d}\tau. \tag{23}$$

By first performing a time-Fourier transform on equation (23) and then making use of equations (12) and (21), we obtain the following expression for the *space–frequency spectrum* $S_{ww}(\mathbf{x}, \mathbf{x}'; \omega)$ of the plate displacement:

$$S_{ww}(\mathbf{x}, \mathbf{x}'; \omega) = \int_{\infty}\int_{\infty}\iint_{\infty}\iint_{\infty} \gamma(\mathbf{x}, \mathbf{x}''; -\omega) S_{p_{b,\Sigma}\, p_{b,\Sigma}}(\mathbf{x}''', \mathbf{x}''; \omega) \gamma(\mathbf{x}', \mathbf{x}'''; \omega)\, \mathrm{d}^2\mathbf{x}''\, \mathrm{d}^2\mathbf{x}''' \tag{24}$$

$$= \int_{\Sigma}\int_{\Sigma}\iint_{\Sigma}\iint_{\Sigma} \gamma(\mathbf{x}, \mathbf{x}''; -\omega) S_{p_b p_b}(\mathbf{x}''' - \mathbf{x}''; \omega) \gamma(\mathbf{x}', \mathbf{x}'''; \omega)\, \mathrm{d}^2\mathbf{x}''\, \mathrm{d}^2\mathbf{x}''', \tag{25}$$

where $S_{p_{b,\Sigma}\, p_{b,\Sigma}}(\boldsymbol{\Xi}; \omega)$ is the *space–frequency spectrum* of the forcing pressure field.

Equation (25) is a classical expression that has been used by many authors to evaluate the response of a fluid-loaded plate to a turbulent wall-pressure [23, 24, 27–31]. However, recent advances in the modelling of turbulence have provided expressions for the wall-pressure fluctuations given in the form of a wavevector–frequency power spectrum [7, 14] and an increasing number of studies are now considering formulations in the wavenumber–frequency domain [11, 13, 32, 33].

According to equation (20), the space–frequency spectrum $S_{p_b p_b}(\boldsymbol{\Xi}; \omega)$ can be expressed in terms of the wavenumber–frequency spectrum $S_{p_b p_b}(\mathbf{k}; \omega)$ as follows:

$$S_{p_b p_b}(\boldsymbol{\Xi}; \omega) = \frac{1}{(2\pi)^2} \int_{-\infty}^{+\infty}\int_{-\infty}^{+\infty} S_{p_b p_b}(\mathbf{k}; \omega) \mathrm{e}^{-\mathrm{j}\mathbf{k}\boldsymbol{\Xi}}\, \mathrm{d}^2\mathbf{k}. \tag{26}$$

When substituted in equations (24) and (25), we recognize the two wavevector–frequency response $\boldsymbol{\Gamma}_{\omega}(\mathbf{k}, \mathbf{k}')$ and the space-varying wavevector-frequency response $\boldsymbol{\Gamma}_{\omega}(\mathbf{x}, \mathbf{k}')$, respectively, defined by

$$\boldsymbol{\Gamma}_{\omega}(\mathbf{k}, \mathbf{k}') = \iint_{\Sigma}\iint_{\Sigma} \gamma(\mathbf{x}, \mathbf{x}'; \omega) \mathrm{e}^{\mathrm{j}(\mathbf{k}\cdot\mathbf{x} + \mathbf{k}'\cdot\mathbf{x}')}\, \mathrm{d}^2\mathbf{x}\, \mathrm{d}^2\mathbf{x}', \tag{27}$$

$$\boldsymbol{\Gamma}_{\omega}(\mathbf{x}, \mathbf{k}') = \iint_{\Sigma} \gamma(\mathbf{x}, \mathbf{x}'; \omega) \mathrm{e}^{\mathrm{j}\mathbf{k}'\cdot\mathbf{x}'}\, \mathrm{d}^2\mathbf{x}', \tag{28}$$

where $\mathbf{k}$ and $\mathbf{k}'$ are, respectively, the Fourier dual variables of the absolute spatial variables $\mathbf{x}$ and $\mathbf{x}'$. It then follows that the space–frequency spectrum (25) of the structural response of

the plate is related to the wavevector–frequency spectrum of the homogeneous excitation field $S_{p_b p_b}(\mathbf{k}; \omega)$ by

$$S_{ww}(\mathbf{x}, \mathbf{x}'; \omega) = \frac{1}{(2\pi)^2} \int_{-\infty}^{+\infty} \int_{-\infty}^{+\infty} \mathbf{\Gamma}_{-\omega}(\mathbf{x}; \mathbf{k}'') S_{p_b p_b}(\mathbf{k}''; \omega) \mathbf{\Gamma}_{\omega}(\mathbf{x}'; -\mathbf{k}'') \, \mathrm{d}^2\mathbf{k}''. \tag{29}$$

Note that $\mathbf{\Gamma}_{\omega}(\mathbf{x}, \mathbf{k}')$ is the space-varying Green function defined in the wavevector–frequency domain and can be interpreted as the *sensitivity* function at position $\mathbf{x}$ of the fluid-loaded plate, to a harmonic excitation with the angular frequency $\omega$ and when the excitation pressure $p_b$ scales on the contribution of the wavevector $\mathbf{k}'$. $\mathbf{\Gamma}_{\omega}(\mathbf{x}, \mathbf{k}')$ is determined by the following system of equations:

$$(\mathscr{L}_P + \mathrm{j}\omega\theta(\omega)\mathscr{L}'_P - m\omega^2)\mathbf{\Gamma}_{\omega}(\mathbf{x}, \mathbf{k}') = -\mathrm{e}^{\mathrm{j}\mathbf{k}'\cdot\mathbf{x}} - [T_{\omega}^{+}(\mathbf{x}, \mathbf{k}') - T_{\omega}^{-}(\mathbf{x}, \mathbf{k}')], \quad \mathbf{x} \in \mathbf{\Sigma}, \tag{30}$$

$$(\mathbf{\Delta} + k_{\pm}^2) T_{\omega}^{\pm}(\mathbf{z}, \mathbf{k}') = 0 \quad \forall \mathbf{z} \in \mathbf{\Omega}^{\pm}, \tag{31}$$

$$\frac{\partial T_{\omega}^{\pm}}{\partial z}(\mathbf{x}, \mathbf{k}') = \rho_{\pm}\omega^2 \mathbf{\Gamma}_{\omega}(\mathbf{x}, \mathbf{k}') \quad \forall \mathbf{x} \in \mathbf{\Sigma}, \tag{32}$$

$$\frac{\partial T_{\omega}^{\pm}}{\partial z}(\mathbf{x}, \mathbf{k}') = 0 \quad \forall \mathbf{x} \in \mathbf{\Sigma}', \tag{33}$$

$$\text{boundary conditions for } \mathbf{\Gamma}_{\omega}(\mathbf{x}, \mathbf{k}') \text{ when } \mathbf{x} \in \partial\mathbf{\Sigma}, \tag{34}$$

$$\text{Sommerfeld radiation conditions for } T_{\omega}^{+} \text{ and } T_{\omega}^{-}. \tag{35}$$

In consequence of definition (27) substituted in equation (24), the *two wavevector–frequency spectrum* $S_{ww}(\mathbf{k}, \mathbf{k}'; \omega)$ of the structural response of the plate is related to the two wavevector–frequency spectrum of the non-homogeneous forcing field $S_{p_b, \Sigma\, p_b, \Sigma}(\mathbf{k}, \mathbf{k}'; \omega)$ by

$$S_{ww}(\mathbf{k}, \mathbf{k}'; \omega) = \frac{1}{(2\pi)^4} \int_{\infty} \int_{\infty} \int_{\infty} \int_{\infty} \mathbf{\Gamma}_{-\omega}(\mathbf{k}', \mathbf{k}'' - \mathbf{k}''') S_{p_b, \Sigma\, p_b, \Sigma}(\mathbf{k}''', \mathbf{k}''; \omega)$$

$$\times \mathbf{\Gamma}_{\omega}(\mathbf{k}' - \mathbf{k}, \mathbf{k}''' - \mathbf{k}'') \, \mathrm{d}^2\mathbf{k}'' \, \mathrm{d}^2\mathbf{k}'''. \tag{36}$$

Expressions (23, 25, 29, 36) are equivalent. They describe, either in the physical domain or in the Fourier domain, the relationship between the statistics of the structural response of a space-limited time-invariant system and the statistics of a random space–time forcing field that can be considered as homogeneous over the plate domain or non-homogeneous over the infinite plane that extends the plate. Figure 2 shows a synoptic diagram which summarizes the methodology we have considered.

### 2.4.2. *Spectral density of the acoustic response*

The *space–frequency spectrum* $S_{p_{\pm} p_{\pm}}(\mathbf{z}, \mathbf{z}'; \omega)$ of the acoustic pressure fields radiated in the fluid domains $\mathbf{\Omega}^{\pm}$ is given by the following expression, which is formally similar

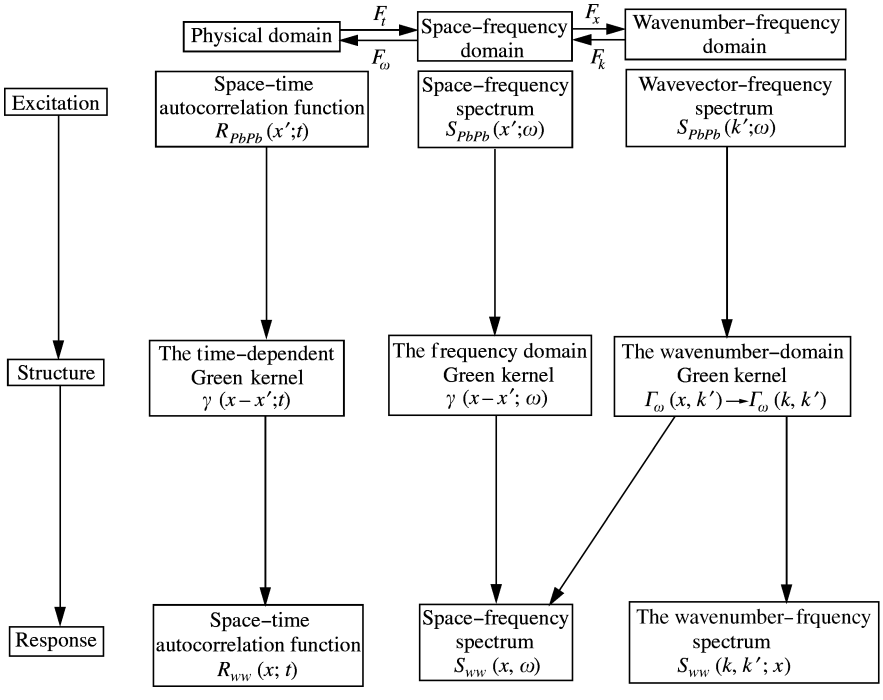


Figure 2. Input–output relationships in the physical or in the Fourier domains with the following notations: $F_t$, time–Fourier transform; $F_\omega$, frequency–Fourier transform; $F_x$, space–Fourier transform; $F_k$, wavenumber–Fourier transform.

to equation (29):

$$S_{p^\pm p^\pm}(\mathbf{z}, \mathbf{z}';\ \omega) = \frac{1}{(2\pi)^2} \int_{-\infty}^{+\infty} \int_{-\infty}^{+\infty} T^{\pm}{}_{\omega}(\mathbf{z}, \mathbf{k}'') S_{p_b p_b}(\mathbf{k}'';\ \omega)\, T_\omega^{\pm *}(\mathbf{z}',\ -\mathbf{k}'')\, \mathrm{d}^2\mathbf{k}'', \quad (\mathbf{z}\ \mathbf{z}') \in \mathbf{\Omega}^\pm. \quad (37)$$

The radiated sound pressure transfer responses $T_\omega^\pm(\mathbf{z}, \mathbf{k}')$ satisfy the set of equations (30–35) and are related to the displacement field by

$$T_\omega^\pm(\mathbf{z}, \mathbf{k}') = \pm\, \rho_\pm \omega^2 \iint_{\mathbf{\Sigma}} \mathscr{G}_\omega^\pm(\mathbf{z} - \mathbf{x}') \mathbf{\Gamma}_\omega(\mathbf{x}', \mathbf{k}')\, \mathrm{d}^2\mathbf{x}'. \quad (38)$$

$\mathscr{G}_\omega^\pm$ are the Green functions of the Helmholtz equation for acoustic propagation in each half-space $\mathbf{\Omega}^+$ or $\mathbf{\Omega}^-$. They satisfy the homogeneous Neumann condition on $(z = 0)$ and the Sommerfeld condition at infinity. They are given by

$$\mathscr{G}_\omega^\pm(\mathbf{z} - \mathbf{z}') = -\frac{\mathrm{e}^{\mathrm{j}k_\pm r(\mathbf{z}, \mathbf{z}')}}{4\pi r(\mathbf{z}, \mathbf{z}')} - \frac{\mathrm{e}^{\mathrm{j}k_\pm r(\mathbf{z}, \mathbf{z}'_-)}}{4\pi r(\mathbf{z}, \mathbf{z}'_-)}, (\mathbf{z}, \mathbf{z}') \in \mathbf{\Omega}^\pm \times \mathbf{\Omega}^\pm, \quad (39)$$

where the co-ordinates of the points $\mathbf{z}'$ and $\mathbf{z}'_-$ are, respectively, $(x', y', z')$ and $(x', y', -z')$. $r(\mathbf{z}, \mathbf{z}')$ denotes the distance between $\mathbf{z}$ and $\mathbf{z}'$.

Expression (38) corresponds to the Green representation of the acoustic pressure transfer responses in the spatial domain. In the wavenumber domain, it reads as

$$T_\omega^\pm(\mathbf{z}, \mathbf{k}') = \pm \frac{\rho_\pm \omega^2}{(2\pi)^2} \left[ \iint_{|\mathbf{k}''| \leqslant k_\pm} \frac{\mathrm{j}\boldsymbol{\Gamma}_\omega(\mathbf{k}'', \mathbf{k}')}{\sqrt{k_\pm^2 - |\mathbf{k}''|^2}} \mathrm{e}^{-\mathrm{j}[\mathbf{k}''\cdot\mathbf{x} \mp z\sqrt{k_\pm^2 - |\mathbf{k}''|^2}]} \, \mathrm{d}^2\mathbf{k}'' \right.$$

$$\left. - \iint_{|\mathbf{k}''| > k_\pm} \frac{\boldsymbol{\Gamma}_\omega(\mathbf{k}'', \mathbf{k}')}{\sqrt{|\mathbf{k}''|^2 - k^2}} \mathrm{e}^{-\mathrm{j}\mathbf{k}''\cdot\mathbf{x}} \mathrm{e}^{\mp z\sqrt{k_\pm^2 - |\mathbf{k}''|^2}} \, \mathrm{d}^2\mathbf{k}'' \right], \quad \mathbf{z} = (\mathbf{x}, z), \quad \mathbf{x} \in \boldsymbol{\Sigma}. \tag{40}$$

This expression is numerically difficult to evaluate and we will prefer to use its spatial counterpart (38) which only involves integrable functions defined over a finite domain. However, the wavevector–Fourier transform (40) simplifies into:

$$T_\omega^\pm(\mathbf{k}, z, \mathbf{k}') = \left\{ \begin{array}{ll} \pm \dfrac{\mathrm{j}\rho_\pm \omega^2 \boldsymbol{\Gamma}_\omega(\mathbf{k}, \mathbf{k}')}{\sqrt{k_\pm^2 - |\mathbf{k}''|^2}} \mathrm{e}^{\pm \mathrm{j}z\sqrt{k_\pm^2 - |\mathbf{k}''|^2}}, & |\mathbf{k}| \leqslant k_\pm \\ \mp \dfrac{\rho_\pm \omega^2 \boldsymbol{\Gamma}_\omega(\mathbf{k}, \mathbf{k}')}{\sqrt{|\mathbf{k}''|^2 - k_\pm^2}} \mathrm{e}^{\mp z\sqrt{|\mathbf{k}''|^2 - k_\pm^2}}, & |\mathbf{k}| > k_\pm. \end{array} \right\}. \tag{41}$$

A formally similar expression will be used in Appendix A of Part II to evaluate the accuracy of our approximations in the simple case of an infinite two-dimensional plate excited by a turbulent boundary layer.

### 2.4.3. *Spectral densities for the power quantities*

In order to obtain the expressions for the spectra associated with the power quantities of interest (input power, radiated acoustic power and structural dissipated power), one needs to establish a power balance equation based upon the weak (energetic) form of the governing equations (2–10).

To this end, equation (2), which is equal to the force per unit area on the panel, is multiplied by the out-of-plane velocity component $\partial w/\partial t(\mathbf{x}'; t + \tau)$ (denoted $\dot{w}$). Evaluating the mathematical expectations (or ensemble averaging) and performing the time–Fourier transform of each term yields the following relationship between several spectral densities in the space–frequency domain:

$$S_{\mathscr{L}_p(w)w}(\mathbf{x}; \omega) + \mathrm{j}\omega\theta(\omega) S_{\mathscr{L}'_p(w)w}(\mathbf{x}; \omega) - m\omega^2 S_{ww}(\mathbf{x}; \omega)$$

$$+ S_{P^+w}(\mathbf{x}; \omega) - S_{P^-w}(\mathbf{x}; \omega) = S_{P_bw}(\mathbf{x}; \omega). \tag{42}$$

The power balance is then obtained by integrating equation (42) over the surface of the plate and by equating the imaginary parts or radiative components of each quantity involved, yielding;

$$S_{\boldsymbol{\Sigma}}(\omega) + S_{\pi^+}(\omega) - S_{\pi^-}(\omega) = S_b(\omega), \tag{43}$$

where $S_{\Sigma}$, $S_{\pi^{\pm}}$ and $S_b$ are, respectively, the structural dissipated power, the acoustic power radiated in $\mathbf{\Omega}^{\pm}$ and the input power. They are determined by the following expressions:

$$S_{\Sigma}(\omega) = \frac{\omega\theta(\omega)}{2} \iint_{\Sigma} S_{\mathscr{L}_p'(w)w}(\mathbf{x};\omega)\,\mathrm{d}^2\mathbf{x}$$

$$= \frac{\eta}{8\pi^2} \iint_{\infty} S_{p_b p_b}(\mathbf{k};\omega) a(\mathbf{\Gamma}_{\omega}, \mathbf{\Gamma}_{\omega})(\mathbf{k})\,\mathrm{d}^2\mathbf{k} \quad \text{(hysteretic damping)}$$

$$= \frac{\sigma\omega}{16\pi^2} \iint_{\infty} S_{p_b p_b}(\mathbf{k};\omega) \langle \mathbf{\Gamma}_{\omega}, \mathbf{\Gamma}_{\omega} \rangle(\mathbf{k})\,\mathrm{d}^2\mathbf{k} \quad \text{(viscous damping)}, \tag{44}$$

where $\sigma$ is a viscous damping force per unit area of the plate and per unit velocity,

$$S_{\pi^{\pm}}(\omega) = \frac{\omega}{2} \Im\left[ \iint_{\Sigma} S_{p^{\pm} w}(\mathbf{x};\omega)\,\mathrm{d}^2\mathbf{x} \right] = \frac{\pm \rho_{\pm} \omega^3}{8\pi^2} \iint_{\infty} S_{p_b p_b}(\mathbf{k};\omega) \beta_{\omega}^{\pm}(\mathbf{\Gamma}_{\omega}, \mathbf{\Gamma}_{\omega})(\mathbf{k})\,\mathrm{d}^2\mathbf{k}, \tag{45}$$

$$S_b(\omega) = \frac{\omega}{2} \Im\left[ \iint_{\Sigma} S_{p_b w}(\mathbf{x};\omega)\,\mathrm{d}^2\mathbf{x} \right] = \frac{\omega}{8\pi^2} \iint_{\infty} S_{p_b p_b}(\mathbf{k};\omega) \Im[\mathbf{\Gamma}_{\omega}^*(\mathbf{k})]\,\mathrm{d}^2\mathbf{k}. \tag{46}$$

Another quantity of interest is the structural response of the system which is characterized by the kinetic energy of the plate, denoted $S_{E_c}(\omega)$. It is given by

$$S_{E_c}(\omega) = \frac{m\omega^2}{2} \iint_{\Sigma} S_{ww}(\mathbf{x};\omega)\,\mathrm{d}^2\mathbf{x} = \frac{m\omega^2}{8\pi^2} \iint_{\infty} S_{p_b p_b}(\mathbf{k};\omega) \langle \mathbf{\Gamma}_{\omega}, \mathbf{\Gamma}_{\omega}^* \rangle(\mathbf{k})\,\mathrm{d}^2\mathbf{k}. \tag{47}$$

The following bi-linear forms have been introduced in expressions (44–46):

$$a(u,v) = \iint_{\Sigma} \left\{ D\left[ \Delta u \Delta v^* + (1-\nu)\left( 2\frac{\partial^2 u}{\partial x \partial y}\frac{\partial^2 v^*}{\partial x \partial y} - \frac{\partial^2 u}{\partial x^2}\frac{\partial^2 v^*}{\partial y^2} - \frac{\partial^2 u}{\partial y^2}\frac{\partial^2 v^*}{\partial x^2} \right) \right] \right.$$
$$\left. - N_x \frac{\partial u}{\partial x}\frac{\partial v^*}{\partial x} - N_y \frac{\partial u}{\partial y}\frac{\partial v^*}{\partial y} \right\}(\mathbf{x})\,\mathrm{d}^2\mathbf{x}, \tag{48}$$

$$\beta_{\omega}^{\pm} = \iint_{\Sigma} \iint_{\Sigma} u(\mathbf{x}) \Im[\mathscr{G}_{\omega}^{\pm}(\mathbf{x} - \mathbf{x}')] v^*(\mathbf{x}')\,\mathrm{d}^2\mathbf{x}\,\mathrm{d}^2\mathbf{x}', \tag{49}$$

$$\langle u, v \rangle = \iint_{\Sigma} (uv^*)(\mathbf{x})\,\mathrm{d}^2\mathbf{x}. \tag{50}$$

The quadratic forms $a(u, u)$, $\beta_\omega(u, u)$ and $\langle u, u \rangle$ are, respectively, proportional to the bending energy of the plate, to the energy radiated by the plate into the fluid and to the kinetic energy of the plate when driven by a harmonic excitation field. In expression (46) for the input power, $\mathbf{\Gamma}_\omega(\mathbf{k})$ is defined by

$$\mathbf{\Gamma}_\omega(\mathbf{k}) = \iint_{\Sigma} \mathbf{\Gamma}_\omega(\mathbf{x}; \mathbf{k}) e^{j\mathbf{k}\cdot\mathbf{x}} d^2\mathbf{x} = \langle \mathbf{\Gamma}_\omega(\mathbf{x}; \mathbf{k}), e^{-j\mathbf{k}\cdot\mathbf{x}} \rangle. \tag{51}$$

It is the spatial Fourier transform of the space-varying wavevector–frequency response of the plate.

Note, from equations (29, 37, 44–47), that the statistics for the response of the system fluid/baffled plate in the space-varying wavevector–frequency domain can be obtained from the spectrum of the excitation $S_{p_b p_b}(\mathbf{k}; \omega)$ passed through a wavevector–frequency filter which is related only to the mechanical and geometrical properties of the system. An equivalent representation of the system response is given by expression (25), but, to our opinion, the interpretation in terms if spatial filters is less intuitive.

In the case of a convecting random pressure field, recent models for turbulence are often formulated using a wavevector–frequency spectrum and this mathematical form can easily be taken into account in expressions (29, 37, 44–47). These expressions are computationally more efficient than those formulated in the space–frequency domain. Indeed, comparing the alternative forms (25) and (29) for the plate displacement, the expression (29) only requires the numerical evaluation of a double infinite integral of a function maximum around the origin $(k_x, k_y) = (0, 0)$, bounded and absolutely integrable over the wavenumber domain. Indeed, this function is represented by the product of two functions: the wavevector sensitivity function, the contribution of the first plate mode which is shown in Figure 3, and the power spectral density of the turbulent boundary layer excitation shown in

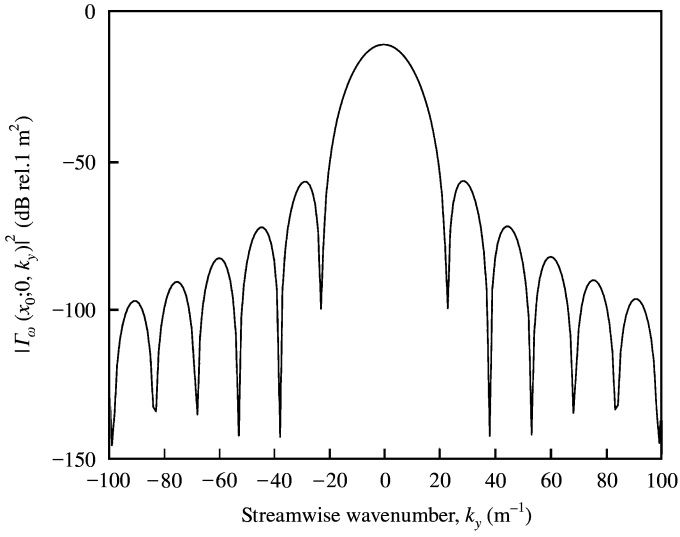


Figure 3. Contribution of the first structural mode to the square modulus $|\mathbf{\Gamma}_\omega(\mathbf{x}_0; 0, k_y)|^2$ of the wavevector sensitivity function calculated at the point $\mathbf{x}_0 = (a/2, b/2)$ on a simply supported plate, as a function of the streamwise wavenumber $k_y$ and for the plate described in section 4.

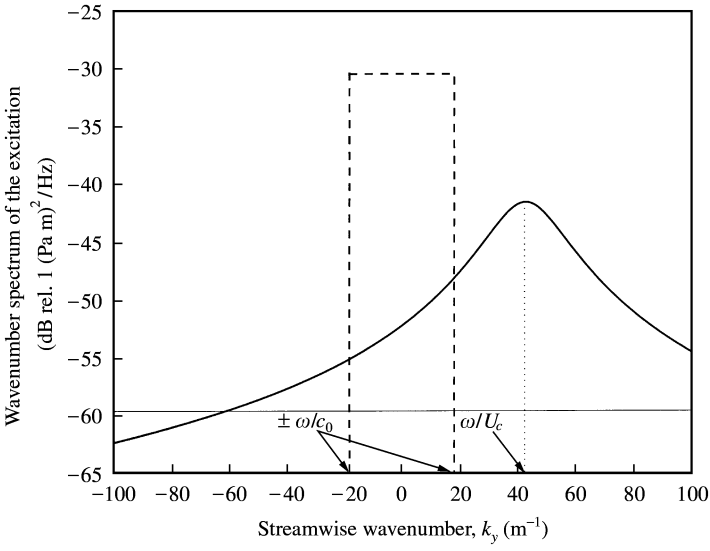


Figure 4. Wavevector spectra for different types of random excitations at $f = 1$ kHz and corresponding to the same root-mean-square wall pressure, as a function of the streamwise wavenumber $k_y$: ——, turbulent boundary layer excitation; - - - -, diffuse field excitation; ——, spatially uncorrelated excitation.

Figure 4 (bold curve). Because the product of these functions drops to zero when $|\mathbf{k}| \to \infty$, as $|\mathbf{k}|^{-6}$ for a simply supported plate and $|\mathbf{k}|^{-8}$ for a clamped plate, the low wavenumber region of the turbulent wall-pressure fluctuations mainly contributes to the system response and so, the infinite integral (29) converges rapidly when approximated by a finite integral defined over an increasing bounded domain centred on the origin and which may easily be evaluated numerically. On the other hand, expression (25) requires the quadruple integration of an oscillating function. It is the combination of all these reasons that justifies our choice of a wavevector–frequency formulation for the response of a flow-excited plate.

The modelling stage of this study has thus led us to the following conclusions. The governing equations of the problem are given by the set of equations (2–10). Because the excitation is not deterministic, the system response is described by random processes characterized, in the wavenumber–frequency domain, by their spectral densities (29, 37, 44–47). It is shown that these spectral densities are obtained from the response of the system to a harmonic deterministic excitation, this latter being evaluated by solving the set of equations (30–35) for each contributing wavenumber $\mathbf{k}$. Thus, the basic problem is to find an efficient method for the determination of the system response to a harmonic excitation. In the next section, we will use an expansion of the system response in terms of its eigenmodes. Since the fluid is a gas, these basis functions will then be approximated by using a perturbation technique.

## 3. EIGENMODES SERIES REPRESENTATION OF THE PANEL RESPONSE

In order to solve the fluid–structure interaction problem described by the set of equations (30–35), many authors [11, 23, 24] expand the fluid-loaded response of the panel as a convergent series of its *in vacuo* eigenmodes. Indeed, the *in vacuo* eigenmodes, as well as the fluid-loaded ones, form a basis of the Hilbert space to which the solution of equations

(30–35) belongs. If the fluid is a gas, the *in vacuo* eigenmodes are quite close to the fluid-loaded structure ones. However, the *fluid-loaded* eigenmodes are much more suitable for estimating the accuracy of the approximations based on neglecting the fluid-loading. Although the coefficient of the fluid-loaded structure modes do not receive any direct physical interpretation, they account exactly for the fluid-loading effects.

As an alternative, the harmonic response of the system fluid/structure can also be expanded as a series of its *resonance modes* or *free oscillation modes*, these latter being approximated by a perturbation technique. It can easily be shown that the zero order terms of this series correspond exactly to the *in vacuo* eigenmodes expansion [22]. The reader interested in this approach may refer to reference [34].

In this section, we will first give the definition of the eigenmodes and eigenfrequencies of the system structure/fluid. We will then show how the harmonic response of the system, and more generally the statistics for the response of the randomly excited panel, can be deduced from the *in vacuo* eigenmodes using an iterative procedure. Finally, we will discuss the conditions under which the modal expansions can be simplified.

### 3.1. EIGENMODE SERIES REPRESENTATION OF THE SYSTEM RESPONSE

The eigenmodes $W_{mn}$ of the fluid/baffled plate system and the corresponding eigenvalues $\lambda_{mn}$ satisfy the homogeneous boundary value problem (30–35) which is equivalent, by use of the Green representation (38), to the following set of integro-differential equations:

$$\mathscr{L}_P(W_{mn})(\mathbf{x};\omega) - \lambda_{mn}(\omega)\left[ W_{mn}(\mathbf{x};\omega) - 2\rho_0/m \iint_{\boldsymbol{\Sigma}} W_{mn}(\mathbf{x}';\omega)\mathscr{G}_\omega(\mathbf{x}-\mathbf{x}')\,\mathrm{d}^2\mathbf{x}' \right] = 0, \quad \mathbf{x}\in\boldsymbol{\Sigma}, \tag{52}$$

$$\text{boundary conditions for } W_{mn}(\mathbf{x};\omega) \text{ when } \mathbf{x}\in\partial\boldsymbol{\Sigma}, \tag{53}$$

where $\lambda_{mn}(\omega) = m\omega_{mn}^2$, $\omega_{mn}$ being the corresponding angular eigenfrequency, and where we assume for clarity that both fluids in $\boldsymbol{\Omega}^+$ and $\boldsymbol{\Omega}^-$ have the same characteristics ($\rho_+ = \rho_- = \rho_0$ and $c_+ = c_- = c_0$). From definitions (48–50), the weak form of equations (52) is given by

$$a(W_{mn}, \delta W) = \lambda_{mn}[\langle W_{mn}, \delta W\rangle - \varepsilon\beta_\omega(W_{mn}, \delta W)], \quad \varepsilon = 2\rho_0/m \tag{54}$$

for any test function $\delta W$ which is twice differentiable, square integrable up to its second derivative and satisfying the same boundary conditions as $W_{mn}$. Because of the radiation condition (35), we note, from definition (52, 53), that the eigenmodes and eigenvalues of the fluid-loaded plate system are frequency-dependent. Moreover, an orthogonality relationship can be deduced from the energetic form (54). After some algebra [22], this leads to the following eigenmodes series expansion for the system response:

$$\boldsymbol{\Gamma}_\omega(\mathbf{x},\mathbf{k}) = \sum_{m,n=1}^{\infty} \frac{\lambda_{mn}}{\lambda_{mn} - m\omega^2} \frac{S_{mn}(\mathbf{k};\omega)}{a(W_{mn}, W_{mn})} W_{mn}(\mathbf{x};\omega), \tag{55}$$

where $S_{mn}(\mathbf{k};\omega)$ is the spatial Fourier transform of $W_{mn}(\mathbf{x};\omega)$.

### 3.2. LIGHT FLUID APPROXIMATION

Inasmuch as the fluid is a gas, the parameter $\varepsilon$ is small and it is numerically efficient to use a perturbation method [35] to build the solution of the problem. To this end, the eigenmodes $W_{mn}$ and the eigenvalues $\lambda_{mn}$ are first sought as Taylor series in the small parameter $\varepsilon$:

$$W_{mn} = W_{mn}^0 + \varepsilon W_{mn}^1 + \varepsilon^2 W_{mn}^2 + \cdots, \quad \lambda_{mn} = \lambda_{mn}^0 + \varepsilon\lambda_{mn}^1 + \varepsilon^2\lambda_{mn}^2 + \cdots. \tag{56}$$

It follows, by substituting expansions (56) into equation (54) and by equating to zero the consecutive powers of $\varepsilon$, that, in particular, the first order terms can be deduced from the zero order terms:

$$\lambda_{mn}^1 = \lambda_{mn}^0 \frac{\beta_\omega(W_{mn}^0, W_{mn}^{0*})}{\langle W_{mn}^0, W_{mn}^{0*}\rangle}, \tag{57}$$

$$W_{mn}^1 = -\sum_{\substack{l,q=1 \\ (l,q)\neq(m,n)}}^{\infty} \frac{\lambda_{mn}^0}{\lambda_{lq}^0 - \lambda_{mn}^0} \frac{\beta_\omega(W_{mn}^0, W_{lq}^{0*})}{\langle W_{mn}^0, W_{lq}^{0*}\rangle} W_{lq}^0, \tag{58}$$

where, for a simply supported plate, the zeroth order approximation of the eigenmodes and eigenfrequencies of the plate are given by

$$W_{mn}^0(x, y) = \sin\left(\frac{m\pi x}{b}\right)\sin\left(\frac{n\pi y}{a}\right), \tag{59}$$

$$\lambda_{mn}^0 = \left\{D\left[\left(\frac{m\pi}{b}\right)^2 + \left(\frac{n\pi}{a}\right)^2\right]^2 + N_x\left(\frac{m\pi}{b}\right)^2 + N_y\left(\frac{n\pi}{a}\right)^2\right\}. \tag{60}$$

An iterative form of higher order approximations can also be obtained, but also involves higher order integration. The intermediate steps of the derivation are detailed in references [22, 35]. Finally, the first order approximation for the eigenmodes series expansion of the system response is given by

$$\mathbf{\Gamma}_\omega(\mathbf{x}, \mathbf{k}') \approx \sum_{m,n=1}^{+\infty} \frac{1}{\tilde{\lambda}_{mn} - m\omega^2} \frac{\tilde{S}_{mn}(\mathbf{k}; \omega)}{\langle W_{mn}^0, W_{mn}^{0*}\rangle} W_{mn}^0(\mathbf{x}), \tag{61}$$

where $\tilde{\lambda}_{mn} = \lambda_{mn}^0 + \varepsilon\lambda_{mn}^1$ and, by denoting $S_{mn}^0$ the spatial Fourier transform of $W_{mn}^0$:

$$\tilde{S}_{mn}(\mathbf{k}; \omega) = S_{mn}^0(\mathbf{k}) + \varepsilon \sum_{\substack{l,q=1 \\ (l,q)\neq(m,n)}}^{+\infty} \frac{1}{\tilde{\lambda}_{mn} - \tilde{\lambda}_{lq}} \left(\frac{\tilde{\lambda}_{mn}}{\tilde{\lambda}_{mn} - m\omega^2} - \frac{\tilde{\lambda}_{lq}}{\tilde{\lambda}_{lq} - m\omega^2}\right) \frac{\beta_\omega(W_{lq}^0, W_{mn}^{0*}) S_{lq}^0(\mathbf{k})}{\langle W_{lq}^0, W_{lq}^{0*}\rangle}. \tag{62}$$

Such an approximation requires some comments. First, as shown in Part II, Appendix A.1 for the case of an infinite plate excited by a TBL, this approximation is valid away from the acoustic coincidence frequency $\omega_c = c_0^2\sqrt{m/D}$ for which the acoustic wavelength matches the bending wavelength associated with the free waves propagating

along the *in vacuo* plate. A uniform expansion of equation (61) as a series of $\varepsilon$ may be obtained by applying the asymptotic matching principle generally used to solve a singular perturbation problem [36].

Second, expansion (61, 62) does not proceed in integral powers of $\varepsilon$, but this form can easily be obtained, when the frequency is not too close to a resonance. For a purely elastic plate, at or near a resonance (say $m\omega^2 \approx \lambda^0_{mn}$), the magnitude of the response is determined by the leading order term which is proportional to $(\mathrm{j}\varepsilon\Im[\lambda^1_{mn}])^{-1}$ and which provides a measure of the radiation damping of the system [37].

Other authors have addressed similar problems [36, 37], but have used different expressions for the fluid-loading parameter $\varepsilon$. This can be explained as follows. We note that dimensioned physical quantities are involved in the set of equations (30–35) which govern the fluid–structure interaction problem. In order to be solved numerically, a reduced form of these equations (54) is often required. To this end, the physical quantities are replaced by their measure in a coherent system of units (length, mass, time), but *the functional form of these equations remains unchanged*. According to the choice of the reference units, either a particular or a wide class of problems can be treated.

In this study, we have chosen the thickness of the plate as a reference for the lengths; the other quantities have been written in a standard unit system. Thus, the dimensionless parameter $\varepsilon = 2\rho_0/m$ measures the ratio between the fluid density and the plate density in a given system of units. As an alternative, Leppington [37] has chosen one acoustic wavelength as a length reference and defined the terms low (or high) fluid loading when $\varepsilon$ is either small (or large) with respect to unity. Furthermore, Crighton [36] has pointed out a unit system such that the parameter $\varepsilon$ is always small, including heavy fluid/structure interaction problems. It is thus interesting to expand the solution as a series of this parameter. However, when these representations are subsequently written in our system of units, one obtains series (61). As a consequence, the relative errors obtained by truncating, at a given order, the asymptotic representations of the solution formulated in different coherent unit systems are always the same.

To complete the asymptotic analysis of our modal formulation, approximate expressions of the power spectral densities of interest will be given. By substituting equation (61) into the wavenumber–frequency spectrum (29) of the plate response, one obtains.

$$S_{ww}(\mathbf{x}, \mathbf{x}'; \omega) \approx \sum_{m,n=1}^{\infty} \sum_{p,q=1}^{\infty} \frac{\boldsymbol{\Psi}^{pq}_{mn}(\omega)}{d_{mn}(\omega) d^*_{pq}(\omega)} \frac{W^0_{mn}(\mathbf{x}) W^0_{pq}(\mathbf{x}')}{N^0_{mn} N^0_{pq}}, \tag{63}$$

where

$$d_{mn}(\omega) = \tilde{\lambda}_{mn}(\omega) - m\omega^2, \quad N^0_{mn} = \langle W^0_{mn}, W^{0*}_{mn} \rangle, \tag{64}$$

and

$$\boldsymbol{\Psi}^{pq}_{mn}(\omega) = \frac{1}{4\pi^2} \iint_{\infty} \tilde{S}_{mn}(\mathbf{k}; \omega) S_{p_b p_b}(\mathbf{k}; \omega) \tilde{S}^*_{pq}(\mathbf{k}; \omega) \, \mathrm{d}^2\mathbf{k}. \tag{65}$$

For the spectral density (45) of the sound power radiated into each fluid domain, it follows that

$$S_{\pi^\pm}(\omega) \approx \pm \frac{\rho_0 \omega^3}{2} \sum_{m,n=1}^{\infty} \sum_{p,q=1}^{\infty} \frac{\boldsymbol{\Psi}^{pq}_{mn}(\omega)}{d_{mn}(\omega) d^*_{pq}(\omega)} \frac{\beta_\omega(W^0_{mn}, W^{0*}_{pq})}{N^0_{mn} N^0_{pq}}. \tag{66}$$

A noteworthy feature for the approximation of the modal formulation related to the other power quantities, in equations (44, 46, 47), is that only a double summation is required, that is

$$S_{\Sigma}(\omega) \approx \frac{\eta\omega}{2} \sum_{m,n=1}^{\infty} \frac{\lambda^0_{mn} \boldsymbol{\Psi}^{mn}_{mn}(\omega)}{|d_{mn}(\omega)|^2 N^0_{mn}}, \tag{67}$$

$$S_b(\omega) \approx \frac{\omega}{2} \sum_{m,n=1}^{\infty} \Im\left[\left(\frac{\boldsymbol{\Psi}^{mn,0}_{mn}(\omega)}{d_{mn}(\omega) N^0_{mn}}\right)^*\right], \tag{68}$$

$$S_{E_c}(\omega) \approx \frac{m\omega^2}{2} \sum_{m,n=1}^{\infty} \frac{\boldsymbol{\Psi}^{mn}_{mn}(\omega)}{|d_{mn}(\omega)|^2 N^0_{mn}}. \tag{69}$$

where

$$\boldsymbol{\Psi}^{mn,0}_{mn}(\omega) = \frac{1}{4\pi^2} \iint_{\infty} \tilde{S}_{mn}(\mathbf{k};\omega) S_{p_b p_b}(\mathbf{k};\omega) S^0_{mn}(\mathbf{k})\, \mathrm{d}^2\mathbf{k}. \tag{70}$$

The above expressions can be further simplified if the eigenmodes in equation (56) are approximated by their zero order terms. If coupling terms are neglected, one obtains the classical *modal representation* of the response of the fluid-loaded system as a series of the plate *in vacuo* eigenmodes.

### 3.3. SIMPLIFICATION IN THE ACOUSTICAL COUPLING

*A priori* criteria can be formulated (see Part II, Appendix A1, expression (A.5)) to evaluate the validity domain of a light fluid approximation if we assume, as suggested in reference [35], that it is of the same order of magnitude for both a finite and an infinite plate. These criteria provide a maximum frequency $\omega_{ac}$ below which the first order terms may be neglected in the approximations (63–70); that is

$$\omega \ll \omega_{ac} = \omega_c[1 - \varepsilon^2_{fl} k^2_b(\omega_c)] \tag{71}$$

with

$$\varepsilon_{fl} = \rho_0 c_0 / m\omega_c. \tag{72}$$

$\varepsilon_{fl}$ is the "intrinsic fluid-loading parameter" introduced by Crighton [36] and corresponds to the ratio $\rho_0/m$ measured in a unit system such that the length unit is the acoustic wavelength at the critical frequency. $k_b$ is the plate bending wavenumber.

If condition (71) is satisfied over the frequency range of interest, then expressions (64, 65) can be replaced by their zero order approximations

$$d_{mn}(\omega) \approx d^0_{mn}(\omega) = \lambda^0_{mn}(\omega) - m\omega^2, \tag{73}$$

$$\boldsymbol{\Psi}^{pq}_{mn}(\omega) \approx \mathring{\boldsymbol{\Psi}}^{pq}_{mn} = \frac{1}{4\pi^2} \iint_{\infty} S^0_{mn}(\mathbf{k}) S_{p_b p_b}(\mathbf{k};\omega) S^{0*}_{pq}(\mathbf{k})\, \mathrm{d}^2\mathbf{k}. \tag{74}$$

We note that, in the literature, expression (73) for the modal resonance coefficient $d_{mn}$ is often written in terms of an equivalent modal damping ratio $\zeta_{mn}$ in the form

$$d^0_{mn}(\omega) = m(-\omega^2 + 2\mathrm{j}\omega\zeta_{mn}\omega^0_{mn} + \omega^{0\,2}_{mn}), \tag{75}$$

where $\omega^0_{mn}$ are the angular eigenfrequencies of the *in vacuo* panel, $\zeta_{mn}$ accounts for the internal damping ($\zeta_{mn} = \eta\omega^0_{mn}/2\omega$), and the energy lost through the panel boundaries, in which case, $\zeta_{mn} = \sigma/m\omega^0_{nm}$ where $\sigma$ has been defined in section 2.4.3.

## 3.4. MODAL ANALYSIS FOR THE STATISTICS OF THE PANEL RESPONSE

The above expressions can be further simplified according to the nature of the forcing field. To illustrate the approach, we consider, in the following, three types of random forcing.

### 3.4.1. *Response to an incidence diffuse field*

We first consider the case in which the panel is excited by an infinite sum of uncorrelated plane waves whose incidence angles are uniformly distributed over a half-space. Because our system is linear, a method of solution, in the physical domain, would be to compute the sensitivity function of the system with $\mathbf{k} = (k_0 \sin\theta\cos\varphi, k_0 \sin\theta \sin\varphi)$ for a discrete set of incidence angles $(\theta, \varphi)$ and ten, to sum the contribution of each incident wave to the system response with a $\sin\theta$ weighting function. In the wavenumber domain, this is equivalent to considering the following form for the spectrum of the excitation.

$$\begin{aligned} S_{p_b p_b}(\mathbf{k};\omega) &= S_0/\pi k_0^2 \quad \text{for } |\mathbf{k}| \leqslant k_0, \quad -\infty < \omega < \infty, \\ &= 0 \qquad\quad \text{for } |\mathbf{k}| > k_0, \quad -\infty < \omega < \infty, \end{aligned} \tag{76}$$

as plotted in Figure 4 (dashed curve). $S_0$ determines the point-power spectral density of the excitation and satisfies the requirement $S_0(\omega) = \iint_\infty S_{p_b p_b}(\mathbf{k};\omega)\,\mathrm{d}^2\mathbf{k}$. In the space–frequency domain, the spatial correlation function associated with (76) has the familiar form $\sin(k_0|\mathbf{x} - \mathbf{x}'|)/k_0|\mathbf{x} - \mathbf{x}'|$ [38].

Under condition (71), the modal excitation term (74) may therefore be written as follows:

$$\mathbf{\Psi}^{pq}_{mn}(\omega) \approx \frac{S_0}{4\pi^3 k_0^2} \iint_{|\mathbf{k}| \leqslant k_0} |\mathbf{k}| S^0_{mn}(\mathbf{k}) S^{0*}_{pq}(\mathbf{k})\,\mathrm{d}^2\mathbf{k}. \tag{77}$$

We note that only the radiating (or supersonic) wavenumber components of the panel eigenmodes are excited by a diffuse field. Equations (63, 66–69) with the approximations (73, 74, 77) have been used for the numerical predictions of the velocity and sound radiation of the plate with an incidence diffuse field.

### 3.4.2. *Response to turbulent wall-pressure fluctuations*

We consider the response of the panel when excited by a weakly stationary and a weakly homogeneous turbulence flowing along the length direction (see Figure 1). The spectrum of the wall-pressure fluctuations is assumed for now to be described by the Corcos model [6],

which can be expressed in the wavenumber domain as

$$S_{p_b p_b}(\mathbf{k};\omega) = \mathbf{\Phi}_0(\omega)\frac{L_x}{[k_x^2 L_x^2 + 1]}\frac{L_y}{[(k_y - \omega/U_c)^2 L_y^2 + 1]} \tag{78}$$

as also plotted in Figure 4 (bold curve). $\mathbf{\Phi}_0(\omega)$ is the point-power spectrum which over the bandwidth considered here (up to 2 kHz) is assumed to be uniform [24], $U_c$ is the convection velocity, $L_x$ and $L_y$ are the correlation lengths and correspond to the distance in the spanwise and streamwise directions over which the wall-pressure fluctuations are strongly correlated. The choice and the interpretation of the Corcos model are discussed in more detail in Part II, section 2, of this paper.

As for the case of an infinite plate (see Part II, Appendix A.2), a criteria can also be formulated for the case of a finite dimensional plate such as the correlation function between the plate displacement and the turbulent forcing field can be further simplified. In particular, such a simplification occurs when the turbulent pressure field is correlated over an area much smaller than the plate surface, i.e., when the plate dimensions are large compared to the correlation lengths [23]. This condition can be written as

$$\begin{aligned} L_x(U_c, \omega) &\ll b, \\ L_y(U_c, \omega) &\ll a, \end{aligned} \tag{79}$$

Requirement (79) defines a transition frequency which, if $L_y = U_c/\alpha_y\omega$, is given by $\omega_T = \mathrm{U}_c/a\alpha_y(\alpha_y \approx 0{\cdot}1$ is a constant derived from experiments). Above this frequency, the cross-terms $\mathring{\mathbf{\Psi}}^{pq}_{mn}$, $((m, n) \neq (p, q))$, in equation (74) can be neglected with respect to the diagonal terms $\mathbf{\Psi}^0_{mn} \equiv \mathring{\mathbf{\Psi}}^{mn}_{mn}$.

If we assume that our frequency range of interest satisfies condition (71) and (79), then spectrum (63) of the plate displacement reduces to

$$S_{ww}(\mathbf{x}, \mathbf{x}';\omega) \approx \sum_{m,n=1}^{\infty} \frac{\mathbf{\Psi}^0_{mn}(\omega)}{|d^0_{mn}(\omega)|^2}\frac{W^0_{mn}(\mathbf{x})W^0_{mn}(\mathbf{x}')}{(N^0_{mn})^2}. \tag{80}$$

Under these conditions, the simplified forms of expressions (66–69) are readily obtained.

### 3.4.3. *Response to a spatially random field*

We now assume that the excitation is white in the wavenumber–frequency domain, i.e., the excitation is completely spatially uncorrelated from one point to another. This excitation corresponds, in the physical domain, to a purely random process, sometimes referred to as "rain on the roof" excitation. An example of this situation in practice would be when we consider the response of a finite membrane excited by the Brownian impact of molecules of the surrounding fluid. Although not strictly physically realizable, this random process is a convenient approximation analyzing the response of a finite system to a broadband wavenumber excitation.

This stationary and homogeneous random process is characterized by a uniform spectral density:

$$S_{p_b p_b}(\mathbf{k};\omega) = S'_0 \quad \text{for all } \mathbf{k}, \omega. \tag{81}$$

It means that the energy content of a purely random field is uniformly distributed over the entire wavenumber–frequency range. However, this definition implies that the mean–square

pressure of such a process is infinite. To overcome this difficulty, this random field is in practice approximated by an ideal low-pass process described by a uniform spectral density defined over a limited wavenumber band, the domain of which is sufficiently large to become a limiting form of a purely random process. In our case, the bandwidth in the wavenumber domain (500 $m^{-1}$) has been chosen so that, given an upper analysis frequency of 2 kHz, it contains all the modes that contribute to the panel response within this frequency range. This bandwidth is closely related to the modal convergence criteria which is presented in Appendix A here.

In this limit and because of the orthogonality relationship between the *in vacuo* eigenmodes of the plate, equation (74), valid under condition (71), then simplifies to:

$$\mathbf{\Psi}_{mn}^{pq}(\omega) \approx S_0'(N_{mn}^0)^2 \delta_{mn}^{pq} \tag{82}$$

and in this case

$$S_{ww}(\mathbf{x}, \mathbf{x}'; \omega) \approx S_0' \sum_{m,n=1}^{\infty} \frac{W_{mn}^0(\mathbf{x}) W_{mn}^0(\mathbf{x}')}{|d_{mn}^0(\omega)|^2}. \tag{83}$$

## 4. NUMERICAL EXAMPLES

Simulations have been carried out to predict, for the three types of random forcing described in the previous section, the response of an untensioned simply supported aluminium panel of dimensions 0·414 × 0·314 × 0·001 m thick, for which the damping ratio is assumed to be constant ($\zeta_{mn} = \zeta = 0{\cdot}01$) in all modes.

In order to compare the panel response for different kinds of random excitations, we have considered the ratio between the power spectral density of the panel response and the point-power spectral density of the excitation. This is equivalent to calculating the power spectral density of the panel response to different types of random excitations, all characterized by a unit point-power spectral density over the frequency bandwidth of interest and so associated to the same mean-square wall pressure $p_{rms}^2$, which is defined in the physical domain as $R_{p_b p_b}(0; 0)$ or, in the wavenumber–frequency domain, as $\int_{-\infty}^{\infty} \iint_{\infty} S_{p_b p_b}(\mathbf{k}; \omega)\, \mathrm{d}^2\mathbf{k}\, \mathrm{d}\omega$.

The wavenumber spectra of a diffuse field, a turbulent boundary layer excitation field and a spatially random excitation field associated with the same mean-square wall pressure are plotted in Figure 4 at a fixed frequency $f = 1$ kHz. For an incidence diffuse field, the energy content is limited to the wavenumber range $[-\omega/c_0, \omega/c_0]$. The weighted distribution of each contributing incident plane wave (due to a higher probability density near the grazing angles of incidence) is described by the model. For a turbulent boundary layer excitation, the main energy fluctuations in the wavenumber spectrum are concentrated around the convecting scales of the flow, i.e., near the convective ridge ($k_x \sim 0$, $k_y \sim \omega/U_c$). The levels of the wavenumber spectrum for the spatially random excitation is low compared to the others since it is flat from $-500$ to 500/m and must have the same mean-square value as above. Figure 5 shows the influence of each kind of excitations on the panel structural response, i.e., on the corresponding normalized spectral densities of the panel kinetic energy $S_{E_c}(\omega)/\iint_{\infty} S_{p_b p_b}(\mathbf{k}; \omega)\, \mathrm{d}^2\mathbf{k}$ (J/Pa$^2$). The bold line is related to a turbulent boundary layer excitation of the panel at a high subsonic Mach number ($M_c = 0{\cdot}77$), the dashed line to an incidence diffuse acoustic field and the thin line, to a purely random field. Figure 6 presents

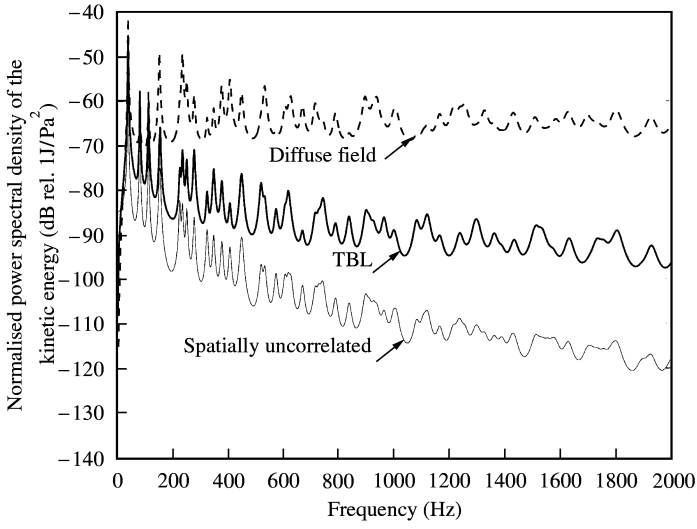


Figure 5. The ratio between the power spectral density of the panel kinetic energy and the point-power spectral density of the excitation as a function of frequency for three types of random forcing: ——, turbulent boundary layer excitation; - - - -, diffuse field excitation; ——, spatially uncorrelated field.

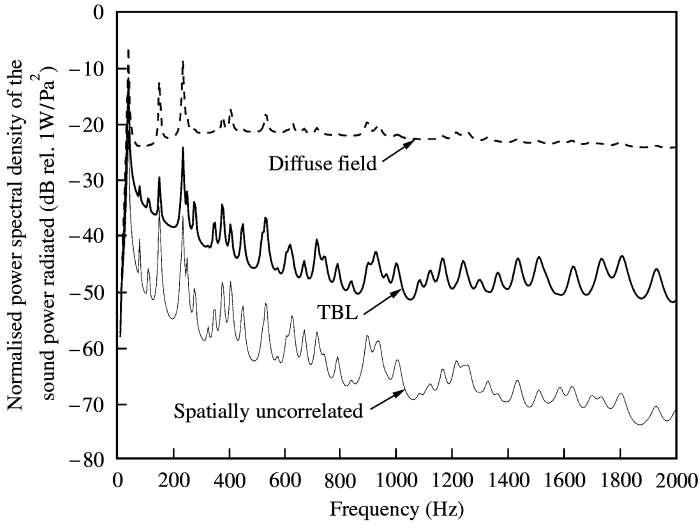


Figure 6. The ratio between the power spectral density of the sound power radiated by the panel and the point-power spectral density of the excitation as a function of frequency for three types of random forcing: ——, turbulent boundary layer excitation; - - - -, diffuse field excitation; ——, spatially uncorrelated field.

the normalized spectra for the radiated acoustic sound power, in the three cases considered above.

Figure 7 represents, in the streamwise wavenumber–frequency domain, the lattice distribution of the panel resonance frequencies together with the hydrodynamic and acoustic coincidence lines. It provides a visual interpretation of the coincidence phenomena.

In order to explain the results shown in Figures 5 and 6, one has to bear in mind that the spectrum levels for the panel structural response will depend on how the system filters the

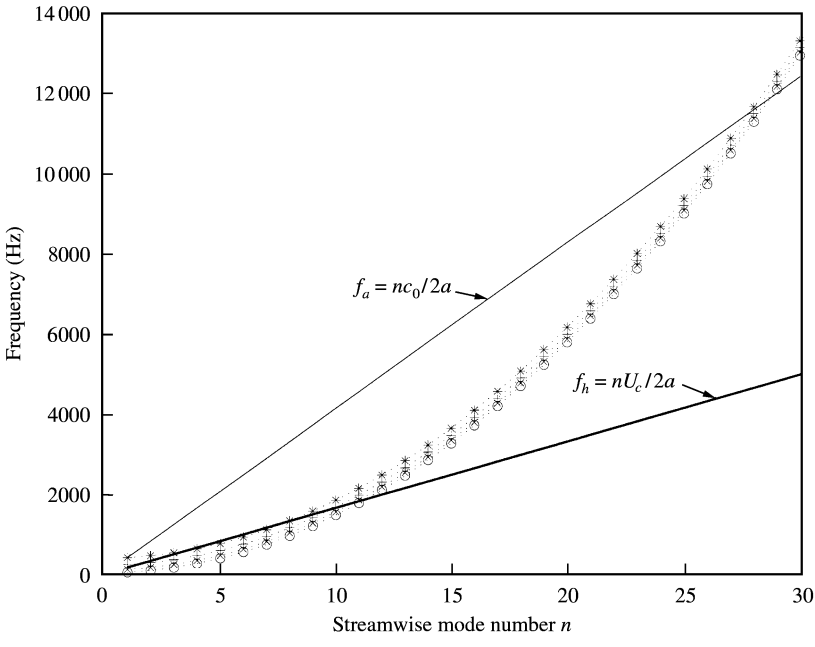


Figure 7. Location of the panel eigenfrequencies in the frequency–streamwise wavenumber domain: —○—, $m = 1$; —×—, $m = 2$; —+—, $m = 3$; —∗—, $m = 4$; ——, hydrodynamic coincidence line ($U_\infty = 225$ m/s); ——, acoustic coincidence line (for $m = 0$).

wavenumber characteristics of the excitation. It is the modal excitation term (79) that describes the wavenumber filtering capabilities of the panel.

For a diffuse acoustic field excitation, a spatial coincidence occurs if the acoustic wavenumber ($k_0 = \omega/c_0$) matches a modal wavenumber ($\sqrt{k_m^2 + k_n^2}$) of the panel. However, below 2 kHz, for the panel of interest, the acoustic wavenumber calculated at the resonant frequency of each structural mode is lower than the corresponding modal wavenumber, as shown in Figure 7, from which it can be seen that the acoustic coincidence frequency occurs at around 11·5 kHz. The modal excitation term (77) calculated at the resonant frequency of each structural mode depends on the supersonic side lobe contribution of each modal sensitivity function $|S^0_{mn}(\mathbf{k})|^2$ in the wavenumber domain. For instance, at 1 kHz, although the (2, 8) mode has its resonance frequency (1001 Hz) closest to the excitation frequency, only the supersonic wavenumber components of this mode match the spacewise variation of the excitation ($\omega_{28}/c_0 = 18{\cdot}5\ \mathrm{m}^{-1}$, $\sqrt{k_2^2 + k_8^2} = 63{\cdot}9\ \mathrm{m}^{-1}$). In this wavenumber range, the modal excitation term also depends on the relative amplitude of the side lobes of each modal sensitivity function and the excitation spectrum $S_{p_b p_b}(\mathbf{k}; \omega)$, which must be borne in mind when comparing this with the influence of a TBL excitation.

For a turbulent boundary layer excitation, the modal excitation term has a maximum value when the convecting scale of the flow (with the corresponding streamwise wavenumber $k_y = \omega/U_c$) is equal to the streamwise modal wavenumber of the panel ($k_n = n\pi/a$): this describes the spatial coincidence phenomenon. Moreover, if the maximum occurs at the resonance frequency of a structural mode (frequency coincidence), then a *hydrodynamic coincidence effect* occurs and cause a large vibrating response of the panel at this frequency. However, as shown in Figure 7, this phenomenon is not highly tuned and, for the configuration of interest and at a high subsonic Mach number ($M_c = 0{\cdot}77$), involves a whole set of modes with their resonance frequencies in the range up to 2 kHz. For

instance, for the frequency at which the excitation spectra have been plotted in Figure 4, the (4, 6) mode of the plate provides the best matching with the turbulent convecting scales ($k_n U_c/\omega = 1{\cdot}05$) and is thus efficiently excited. However, a large response due to resonant amplification does not occur because its resonance frequency (900 Hz) is not close to the excitation frequency. On the other hand, resonant modes are not necessarily those which are the most efficiently excited. As shown in Figure 7, it appears that most of the modes that contribute to the panel response in the hydrodynamic coincidence region are non-resonant, but efficiently excited modes. Above the hydrodynamic coincidence area, these non-resonant modes still contribute to the off-resonant response of the panel, but the relative contribution of resonant and weakly excited mode increases with frequency.

When comparing the influence of a TBL excitation and a diffuse field on the panel vibro-acoustic response for a given mean-square pressure level in Figures 5 and 6, we notice that, up to 2 kHz, the levels for the vibrating response of the panel excited by a diffuse field are higher by up to 20–25 dB than those observed for a TBL excitation. This is directly related to the difference levels observed in Figure 4 between the diffuse field and the TBL excitation spectra in order to reproduce the same mean-square pressure. It implies that, up to 2 kHz, the separation distance beyond which the random fluctuations due to the diffuse field may be regarded as completely uncorrelated over the plate is greater than the correlation lengths associated to the turbulent fluctuations. It also implies that the modes that contribute to the panel response under a diffuse field excitation are more efficiently excited than in the case of a TBL excitation.

In summary, for a given mean-square wall pressure and in the low-frequency domain, the panel modes have a better coupling with a diffuse field excitation than with a turbulent boundary layer excitation that, in turn, excites more efficiently the structural modes of the panel than a purely random field. For a diffuse excitation, the forcing field couples well with different panel modes whereas, for a TBL excitation at a high subsonic Mach number and for a purely random field, the panel modes are uncorrelated (the cross modal excitation terms are negligible with respect to the diagonal terms). The influence of resonant (frequency coincident) and non-resonant modes can also be studied. For a diffuse field, a large proportion of non-resonant modes and resonant modes are efficiently excited over a broad frequency range below the acoustic coincidence frequency. A similar situation occurs for a TBL excitation, but below the hydrodynamic coincidence frequency. For a purely random field, only the resonant terms have a dominant role, especially in the very low-frequency domain.

A more detailed analysis of the response of an aircraft panel to a turbulent flow is carried out, using a wavenumber approach, in section 3 of Part II. In Appendix A here, the convergence of the modal approach is considered for the three type of random excitations.

## 5. CONCLUSION

A general and self-contained model is presented for predicting both the vibrating response and the acoustic radiation of a thin baffled plate stressed by in-plane tensions and excited by a large class of random fields. The spectral densities of the system response are expressed, in the wavevector–frequency domain, in terms of the spectral density of the turbulent excitation "filtered" by the sensitivity function of the plate. This latter quantity can be computed once for all excitations and is *a priori* independent of the nature of the excitation field. In practice, it is deduced from the system response to a harmonic excitation with a spatial dependence scaled on each contributing wavevector. The sensitivity function can be expressed as a series of eigenmodes for the fluid-loaded system and a perturbation

method has been applied in order to take advantage of the weak influence of the surrounding fluid on the vibro-acoustic response of the system. A *priori* physical criteria have been proposed to simplify these expressions. These approximations assume the acoustic modal coupling to be neglected well below the acoustic coincidence frequency and, for a convecting random field, the cross-modal excitation terms can be neglected above a certain frequency. They will be verified in Part II of this paper in the case of an aircraft fuselage panel excited by a turbulent flow.

Modal series have been derived for the statistical properties of the panel response to three types of random excitation and which has been calculated as a function of frequency for a given mean-square wall pressure. Several trends have been pointed out: (i) the panel structural modes are more efficiently excited with an incidence diffuse field than with the wall-pressure fluctuations due to a turbulent boundary layer whereas a turbulent excitation couples better with the panel modes than a purely random field; (ii) under a diffuse field excitation, the structural modes do not contribute independently to the panel response; they can be considered as uncorrelated for a turbulent excitation at high subsonic Mach number; the same conclusion applies for a spatially random field; (iii) both resonant and non-resonant modes contribute to the panel response over a broad frequency range, below the acoustic coincidence frequency for a diffuse field excitation, and over the hydrodynamic coincidence area for a turbulent excitation; for a purely random field and in the low modal density region, only the resonant modes have a dominant role.

The convergence properties of the modal series for the vibrating and acoustic response of the system have also been examined and criteria have been formulated to estimate the accuracy of the modal approximations according to the nature of the excitation. For a purely random or a high subsonic turbulent excitation, accounting for mode with resonant frequencies up to the upper analysis frequency is sufficient to ensure adequate convergence of the modal series. However, for an incidence diffuse field, composed of an infinity of independent plane waves, it is not clear above which frequency the cross-modal excitation terms can be neglected. We have shown that this modal coupling has a beneficial effect on the number of modes required to model the structural response of the system (below the acoustic coincidence frequency), but one then has to be careful when dealing with the acoustic response of the system.

## ACKNOWLEDGMENTS

The author would like to thank the anonymous reviewers for their helpful and insightful comments. The first author was supported by EPSRC grant no. N21529.

## REFERENCES

1. W. A. Strawderman 1990. *Naval Underwater Systems Center Technical Document No.* 008-047-00408-7. Wavevector–frequency analysis with applications to acoustics.
2. G. Maidanik and D. W. Jorgensen 1967 *Journal of the Acoustical Society of America* **42**, 494–501. Boundary wave-vector filters for the study of the pressure field in a turbulent boundary layer.
3. W. K. Blake and D. M. Chase 1971 *Journal of the Acoustical Society of America* **49**, 862–877. Wavenumber–frequency spectra of turbulent boundary layer pressure measured by microphone arrays.
4. F. A. Aupperle and R. F. Lambert 1972 *Journal of Sound and Vibration* **24**, 259–267. On the utilization of a flexible beam as a spatial filter.

5. N. C. MARTIN and P. LEEHEY 1977 *Journal of Sound and Vibration* **52**, 95–120. Low wavenumber wall pressure measurements using a rectangular membrane as a spatial filter.
6. G. M. CORCOS 1963 *Journal of the Acoustical Society of America* **35**, 192–199. Resolution of pressure in turbulence.
7. D. M. CHASE 1980 *Journal of Sound and Vibration* **70**, 29–67. Modelling the wavevector–frequency spectrum of turbulent boundary layer wall-pressure.
8. J. E. FFOWCS WILLIAMS 1982 *Journal of Fluid Mechanics* **125**, 9–25. Boundary-layer pressures and the Corcos model: a development to incorporate low-wavenumber constraints.
9. A. V. SMOL'YAKOV and V. M. TKACHENKO 1992 *Soviet Physics Acoustics* **37**, 627–631. Model of a field of pseudosonic turbulent wall pressures and experimental data.
10. F. A. AUPPERLE and R. F. LAMBERT 1973 *Journal of Sound and Vibration* **26**, 223–245. Acoustic radiation from plates excited by flow noise.
11. W. R. GRAHAM 1996 *Journal of Sound and vibration* **192**, 101–120. Boundary layer induced noise in aircraft, Part I: the flat plate model.
12. F. HAN, R. J. BERNHARD and L. G. MONGEAU 1999 *Journal of Sound and Vibration* **227**, 685–709. Prediction of flow-induced structural vibration and sound radiation using energy flow analysis.
13. A. O. BORISYUK and V. T. GRINCHENKO 1997 *Journal of Sound and Vibration* **204**, 213–237. Vibration and noise generation by elastic elements excited by a turbulent flow.
14. W. R. GRAHAM 1997 *Journal of Sound and Vibration* **206**, 541–565. A comparison of models for the wavenumber–frequency spectrum of turbulent boundary layer pressures.
15. A. V. SMOL'YAKOV and V. M. TKACHENKO 1983 *The Measurement of Turbulent Fluctuations*: *An Introduction to Hot-Wire Anemometry and Related Transducers*. Berlin: Springer-Verlag.
16. Y. K. LIN 1967 *Probabilistic Theory of Structural Dynamics*. New York: McGraw-Hill Book Company.
17. PH. MORSE and H. FESHBACH 1953 *Methods of Theoretical Physics*. New York: McGraw-Hill Book Company.
18. A. PREUMONT 1994 *Random Vibration and Spectral Analysis. Solid Mechanics and its Applications*. Dordrecht, The Netherlands: Kluwer Academic Publishers.
19. M. C. JUNGER and D. FEIT 1993 *Sound, structures and their interaction*. Acoustical Society of America (1972 and 1986 by the Massachusetts Institute of Technology).
20. M. J. LIGHTHILL 1952 *Proceedings of the Royal Society of London* **211**, On sound generated aerodynamically. I. General theory.
21. R. L. CLARK and K. D. FRAMPTON 1997 *Journal of the Acoustical Society of America* **102**, 1639–1647. Aeroelastic structural acoustic coupling: implications on the control of turbulent boundary-layer noise transmission.
22. D. HABAULT and P. J. T. FILIPPI 1999 *Journal of Sound and Vibration* **213**, 333–374. Light fluid approximation for sound radiation and diffraction by thin elastic plates.
23. H. G. DAVIES 1971 *Journal of the Acoustical Society of America* **55**, 213–219. Sound from turbulent boundary layer excited panels.
24. G. ROBERT 1984 *Thèse No*. 84-02, *Ecole Centrale de Lyon*, *France*. Modélisation et simulation du champ excitateur induit sur une structure par une couche limite turbulente.
25. G. K. BATCHELOR 1953 *The Theory of Homogeneous Turbulence*. (Reissued in the Cambridge Science Classics series 1982) Cambridge University Press).
26. S. H. CRANDALL 1970 *Journal of Sound and Vibration* **11**, 3–18. The role of damping in vibration theory.
27. I. DYER 1959 *Journal of the Acoustical Society of America* **31**, 922–928. Boundary layer induced flow noise.
28. S. BANO, R. MARMEY, L. JOURDAN and J.-P. GUIBERGIA 1992 *Journal d'Acoustique* **5**, 99–124. Etude théorique et expérimentale de la réponse vibro-acoustique d'une plaque couplée à une cavité en fluide lourd.
29. P. J. T. FILIPPI and D. MAZZONI 1994 In *Boundary Elements XVI* (C. A. Brebbia, editor), 47–54. Southampton-Boston: Computational Mechanics Publications. Noise induced inside a cavity by an external turbulent boundary layer.
30. D. R. THOMAS and P. A. NELSON 1995 *Journal of the Acoustical Society of America* **98**, 2651–2662. Feedback control of sound radiation from a plate excited by a turbulent boundary layer.
31. C. DURANT, G. ROBERT, P. J. T. FILIPPI and P.-O. MATTEI 2000 *Journal of Sound and Vibration* **229**, 1115–1155. Vibroacoustic response of a thin cylindrical shell excited by a turbulent internal flow: comparison between numerical prediction and experimentation.

32. Y. F. HWANG and G. MAIDANIK 1990 *Journal of Sound and Vibration* **142**, 135–152. A wavenumber analysis of the coupling of a structural mode and flow turbulence.
33. D. MAZZONI and U. KRISTIANSEN 1999 *Flow, Turbulence and Combustion* **61**, 133–159. Finite-difference method for the acoustic radiation of an elastic plate excited by a turbulent boundary layer: a spectral domain solution.
34. P. J. T. FILIPPI, D. HABAULT, P.-O. MATTEI and C. MAURY 2001 *Journal of Sound and Vibration* **239**, 639–663. The role of the resonance modes in the response of a fluid-loaded structure.
35. P. J. T. FILIPPI, P.-O. MATTEI, C. MAURY, A. H. P. VAN DER BURGH and C. J. M. DE JONG 2000. *Journal of Sound and Vibration* **229**, 1157–1169. Sound transmission through a thin baffled plate: validation of a light fluid approximation with numerical and experimental results.
36. D. G. CRIGHTON, A. P. DOWLING, J. E. FFOWCS WILLIAMS, M. HECKL and F. G. LEPPINGTON 1992 *Modern Methods in Analytical Acoustics. Lecture notes* Berlin: Springer-Verlag.
37. F. G. LEPPINGTON 1976 *The Quarterly Journal of Mechanics and Applied Mathematics* **XXIX**, 527–546. Scattering of sound waves by finite membranes and plates near resonance.
38. H. NELISSE, O. BESLIN and J. NICOLAS 1996 *Journal of Sound and Vibration* **198**, 485–506. Fluid-structure coupling for an unbaffled elastic panel immersed in a diffuse field.
39. C. MAURY, P. GARDONIO and S. J. ELLIOTT 2000 *ISVR Technical Report No.* 287. Model for the control of the sound radiated by an aircraft panel excited by a turbulent boundary layer.
40. D. GOTTLIEB and S. A. ORSZAG 1977 *Regional Conference Series in Applied Mathematics, CBMS-NSF* 26. Philadelphia: Society for Industrial and Applied Mathematics. Numerical analysis of spectral method: theory and applications.
41. W. K. BLAKE 1986 *Mechanics of Flow-Induced Sound and Vibration: Complex Flow-Structure Interactions*, II. New York: Academic Press.

## APPENDIX A: CONVERGENCE STUDY

It is important to consider the accuracy of the approximation in relation to the finite number of modes retained in the modal approach. We have noted in section 4 that, for a TBL excitation for instance, the plate response is mainly governed by both the resonant and non-resonant modes that are efficiently excited over the hydrodynamic frequency range. The number of resonant modes whose eigenfrequencies fall within a frequency range can always be determined. The main difficulty is to estimate the number of non-resonant modes that will contribute significantly in the modal representation (63) of the solution because they are highly excited. As discussed in reference [39], this is governed by the bandwidth of the excitation field. Indeed, under approximation (71), the excitation spectrum $S_{p_b p_b}$ can be expanded as a series of the *in vacuo* eigenmodes, or structural modes, as follows:

$$S_{p_b p_b}(\mathbf{x}, \mathbf{x}'; \omega) \approx \sum_{m,n=1}^{\infty} \sum_{p,q=1}^{\infty} \mathring{\mathbf{\Psi}}_{mn}^{pq}(\omega) W_{mn}^{0}(\mathbf{x}) W_{pq}^{0}(\mathbf{x}'). \tag{A.1}$$

The non-resonant modes which have a negligible contribution in the excitation representation (A1) will have a negligible contribution in the system response with the general expression (63). This formulation provides an efficient method of determining the required number of highly excited and non-resonant modes in equation (63) since expansion (A1) is readily obtained once the excitation model is known. We note that this methodology can be applied whatever the nature of the excitation and generalized to the case of fluid-loaded eigenmodes or resonance modes. However, more specific rules of convergence can also be derived according to the nature of the excitation.

To study the convergence of the modal series, we use as an estimator the relative error between the truncated modal expansion of the solution and an approximation of the solution when accounting for a sufficient number of modes for the series to converge. In order to obtain a simple estimation of the error in the solution when we account for an

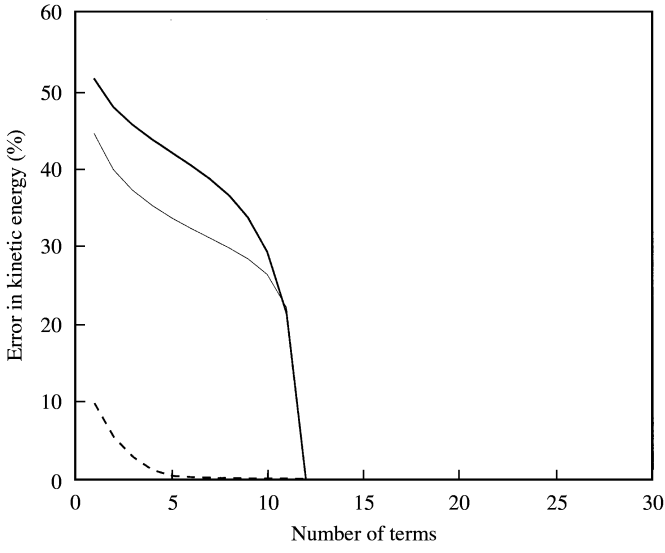


Figure A1. Comparison of percentage errors at $f = 2$ kHz as a function of the number of terms in the modal summation for the panel kinetic energy: ——, turbulent boundary layer excitation; - - - -, diffuse field excitation; ——, spatially uncorrelated excitation.

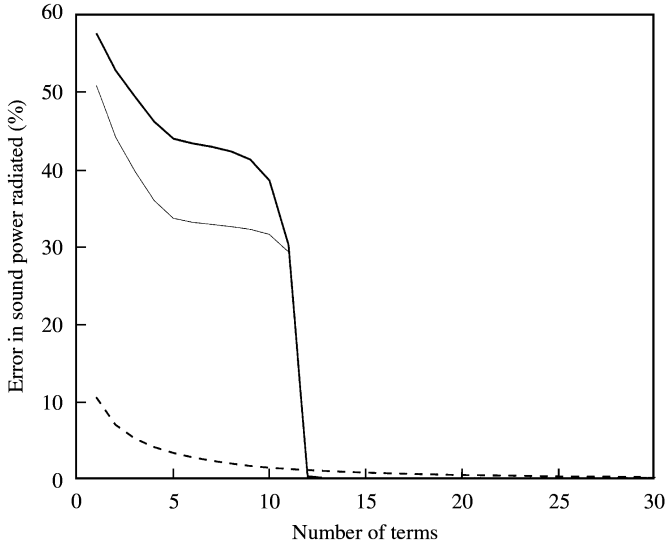


Figure A2. Comparison of percentage errors at $f = 2$ kHz as a function of the number of terms in the modal summation for the sound power radiated by the panel: ——, turbulent boundary layer excitation; - - - -, diffuse field excitation; – – – –, spatially uncorrelated excitation.

increasing number of modes, the following simulations have been carried out on a one-dimensional plate whose length is equal to the panel length. The percentage error at 2 kHz for an increasing number of terms in the modal series is plotted in Figures A1 and A2 for the kinetic energy and the sound power radiated and for the three types of excitations. In Figure 8, as the number of terms increases, the error for a turbulent excitation (bold line) and for a purely random excitation (thin line) both collapse towards zero just before the

number of terms required to reach convergence whereas the error for the diffuse field (dashed line) converges earlier towards zero, but at a lower rate.

A simple criterion can be formulated in the general case to determine the number, $N_{max}$, of structural modes required for convergence of the modal series up to a fixed frequency $f$. Convergence is reached when the distance between two nodes of the structural mode shape is less or equal than the half-wavelength $\lambda_b/2$ of the bending wave on the plate at the analysis frequency, that is, of the function to approximate. It reads as

$$a/N_{max} \leqslant \lambda_b(\omega)/2, \tag{A.2}$$

where $a$ is a plate dimension, or

$$N_{max} \geqslant a(m/D)^{1/4}\sqrt{\omega/\pi^2}, \tag{A.3}$$

where $\lambda_b(\omega) = 2\pi(D/m)^{1/4}\omega^{-1/2}$. Criteria (A.3) is based on the assumption that the structural modes contribute independently to the system response at the frequency of interest. This is obvious when the system is excited by a spatially random field and, for a turbulent excitation, this is justified through condition (79). Thus, for $f = 2\,\text{kHz}$ with $a = 0{\cdot}414\,\text{m}$ for the plate used here, one obtains $N_{max} \geqslant 12$. This is in agreement with the results presented in Figure A1.

For an incidence diffuse field, the situation is somewhat different because the excitation couples with different structural modes. Performing expansion (A.1) of the correlation function for a diffuse sound field (with the typical form $\sin(k_0|\mathbf{x} - \mathbf{x}'|)/k_0|\mathbf{x} - \mathbf{x}'|$) in terms of the plate *in vacuo* eigenmodes (59), it can be shown that, in order to reach convergence, the smallest wavelength of the "trigonometric functions" must be less or equal to the acoustic wavelength at the frequency of interest [40]. It suggests that the number $N_{max}$ of modal functions required to reach convergence at the angular frequency $\omega$ is such that

$$N_{max} \geqslant a\omega/\pi c_0. \tag{A.4}$$

We note that, since, in this example, the analysis frequency is well below the acoustic coincidence frequency, the coupling due to the diffuse field between different modes has a beneficial effect on the convergence properties of the approximate solution with respect to the convergence properties related to a white or a turbulent excitation (see Figure A1).

Criteria (A.4) leads to $N_{max} \geqslant 5$ at $f = 2\,\text{kHz}$, which is in accordance with the results presented in Figure A1. At higher frequencies at or near the acoustic coincidence frequency, criteria (A.3) and (A.4) provide the same number of modes for convergence, but, in this frequency range, a modal formulation of the system response may not be appropriate.

For each kind of excitation, Figure A2 compares the convergence properties for the power spectral densities of the sound power radiated. Although the convergence rates are slightly degraded for the approximation of the sound power radiated by the panel with respect to the approximation of its kinetic energy for a spatially white or a turbulent excitation, the convergence is obtained for the same number of modes. On the other hand, for a diffuse excitation field, a higher number of modes have to be accounted for in order to reach the convergence limit for the approximation of the sound power radiated with respect to the approximation of the kinetic energy.

In the case of a spatially random excitation, the results can be understood since, at 2 kHz, higher order modes are non-resonant and weakly excited modes. Because they do not

couple, via the excitation, with low order resonant but still weakly excited modes, they do not contribute to the vibro-acoustic response of the system. In the case of TBL and diffuse field excitations, the results require some comments.

In general, when low and high order inefficient modes are both highly excited, we can expect a better convergence in the acoustic response than in the structural response since high order inefficient modes have smaller radiation efficiencies than low order modes. The modal series for which the convergence results are presented have been calculated at 2 kHz. In our configuration and in the case of a TBL excitation, this frequency is very close to the hydrodynamic coincidence frequency for which the number of resonant modes in coincidence is maximum. It is found that these modes are mostly inefficient "edge modes" with low spanwise modal order, but which are still more efficient radiators than "corner modes" with the same streamwise modal order [41]. The higher order modes included in the series are mainly non-resonant and weakly excited modes and so, they have a negligible contribution to the panel kinetic energy. Because these modes are mostly corner modes which are very inefficient radiators, they do not significantly modify the acoustic response of the panel if they are accounted for in the modal series. However, some higher order modes are also edge modes which have above average radiation efficiency at 2 kHz. It results in a lower convergence rate for the acoustic response of the panel with respect to its vibrating response.

As noted in section 4, a diffuse sound field efficiently excites supersonic edge modes, but also couples with the supersonic side lobe contribution of subsonic edge modes and, to a much lesser extent, with the supersonic side lobe contribution of some low order corner modes. Below the coincidence frequency, the subsonic corner modes which are resonant contribute significantly to the panel kinetic energy. However, the contribution of the edge modes to the radiated sound cannot be neglected with respect to the corner modes contribution and so, a higher number of mode is required to accurately describe the acoustic response with respect to the structural response.

As a final remark, we note that, according to the nature of the excitation, some quantities can be formulated using a modal summation that do not converge to a limit for an increasing number of modes. This is the case, for instance, for the frequency-integrated "total" kinetic energy $T_{E_c}$ of the panel under a spatially random excitation. This latter quantity is defined by

$$T_{E_c} = \int_{-\infty}^{+\infty} S_{E_c}(\omega)\,\mathrm{d}\omega. \tag{A.5}$$

For a spatially random excitation, it may be written as

$$T_{E_c} \approx \frac{m}{2} \sum_{m,n=1}^{\infty} \int_{-\infty}^{+\infty} \frac{\omega^2}{|d^0_{mn}(\omega)|^2}\,\mathrm{d}\omega = \frac{\pi}{4m} \sum_{m,n=1}^{\infty} \frac{1}{\zeta_{mn}\omega_{mn}} = \frac{\pi}{4} \sum_{m,n=1}^{\infty} \frac{1}{\sigma}. \tag{A.6}$$

The quantity $\zeta_{mn}\omega_{mn}$ is the modal bandwidth of the $(m, n)$ mode of the panel. It can be related to the constant viscous damping force $\sigma$ per unit area of the panel and per unit velocity and so, series (A.6) does not converge. Each term of this series represents the contribution of one mode to the total kinetic energy and, since the energy is uniformly distributed between the modes, the total kinetic energy is unbounded.

For a turbulent excitation, we have shown that the main part of the kinetic energy is concentrated around the modes with a wavelength matching the boundary layer convecting scales. Moreover, the maximum level for the modal excitation terms decreases as $N_{max}^{-l}(l > 1)$, thus ensuring the convergence of the modal series for the total kinetic energy of the panel. For a diffuse field excitation, numerical simulations have shown that the modal series is again convergent, as expected.